Final Project Report under the
Remote Sensing Portion of the
NASA Institutional Grant to
The University of Wisconsin
1969-1970

ATMOSPHERIC EFFECTS ON REMOTE SENSING

by

Alfred J. Stamm and Thomas H. Vonder Haar

Space Science and Engineering Center
The University of Wisconsin
Madison, Wisconsin 53706

August 15, 1970

Project No. 100823; T. H. Vonder Haar, Principal Investigator

Final Project Report under the
Remote Sensing Portion of the
NASA Institutional Grant to the
University of Wisconsin
1969-1970

ATMOSPHERIC EFFECTS ON REMOTE SENSING

by

Alfred J. Stamm and Thomas H. Vonder Haar

Space Science and Engineering Center

University of Wisconsin

Madison, Wisconsin 53706

August 15, 1970

Project No. 100823; T. H. Vonder Haar, Principal Investigator

Abstract

An introductory discussion of the various phenomena which take place in the atmosphere effecting visible and infrared radiation is given. Included are absorption and emission, scattering, and local changes of the index of refraction of the air, and how they effect intensity, contrast, spectral signature, and distortion. Many examples are presented including 48 Figures and 7 Tables. The purpose of this paper is to make the reader aware of atmospheric-induced problems encountered in remote sensing of earth surface features. Forty-one references are given to more complete work.

ATMOSPHERIC EFFECTS ON REMOTE SENSING

TABLE OF CONTENTS

ATMOSPHERIC EFFECTS ON REMOTE SENSING

I. Introduction

The purpose of this paper is to familiarize engineers and earth scientists interested in remote sensing of surface features with some atmospheric effects on their measurements; to aid them in gaining a primary understanding of these effects; and to direct them to more detailed discussions, if necessary.

The atmosphere effects visible and infrared electromagnetic radiation in three primary ways: absorption and emission, scattering, and local changes in the index of refraction of the air. These phenomena cause changes in the intensity, contrast, spectral signature, and apparent source locations of the objects being viewed (distortion). This paper will present an introductory discussion of the phenomena, as well as some simple examples of the resulting effects. (References will be given to more detailed work). Once the reader is aware of the problems, he can consider the conditions of an experiment in the light of possible effects on his results. These will vary, of course, as more atmosphere is placed between detector and target; as one moves from a stepladder to an aircraft to a satellite.

Since this paper is meant to deal only with how the atmosphere effects electromagnetic radiation, the sources and detectors of radiation will not be discussed. The reader is directed to a book such as Kruse, et al., (1962) for such information. Nicodemus (1963) gives a good summary of Radiometric Units. The most important of these are given in Table I.

2. The Atmosphere

The atmosphere consists of several layers delineated by atmospheric properties which vary with height in a generally regular manner. The most common framework is that due to the thermal structure (see Figure 1). In the lowest 10 km called the troposphere, the temperature decreases roughly linearly with height since the atmosphere is primarily heated by the ground. Above this the temperature levels off and then increases again due to ultraviolet light absorption by the concentration of ozone at this altitude. This atmospheric region is called the stratosphere. At about 50 km the temperature starts to decrease again and this layer is called the mesosphere. At still higher altitudes, over about 80 km, the molecules are so far apart that thermodynamic equilibrium does not exist and the temperature of the individual molecules starts to rise again. This region is called the thermosphere (U.S. Standard Atmosphere, 1962).

As warm air rises, it expands due to the lower pressure at higher altitude, and therefore cools. As long as the surrounding atmosphere also cools with height at a proper rate, the air parcel can continue to rise. The water vapor in the air parcel condenses since the cooler air has a lower saturation point. This is what forms clouds. Since the air parcel must be able to rise, water vapor clouds are limited to the troposphere. They can also exist in the mesosphere (noctilucent clouds) but are more rare since there is not much water vapor there.

The atmosphere is made up of oxygen and nitrogen plus a number of minor gasses, some fixed and some variable in concentration (see Figure 2). The minor gasses which are important in absorption will be dealt with in that section: here, only water will be mentioned. Water can be found in any of its

three phases in the atmosphere and its concentration varies both spatially and temporally. Since most remote sensing is done in the absence of clouds, only water vapor is of great importance here; however, both ice and water clouds will change the intensity and spectrum of natural illumination. This will be discussed further after analyzing the phenomena of absorption and scattering.

Besides gasses, the atmosphere contains many kinds of aerosols, from salt over the oceans and dust over deserts to ash from fires and volcanoes as well as the many man-induced pollutants. The effects of these aerosols are only beginning to be studied extensively; a few of the results will be given later in this paper.

Since, as will be shown, remote sensing depends on the present weather (temperature, pressure, moisture, winds, and cloudiness) as well as previous weather (rainfall and winds especially in determining aerosol content), it is important that control areas be viewed, in each region that flights are made and each time a flight is made, in order to allow even relative comparison of measurements obtained under different atmospheric conditions.

3. Absorption

Electrons in atoms are located in certain definite energy levels. When an electron jumps from an outer shell or high energy state to an inner shell or low energy state, visible or ultraviolet light is emitted depending on the energy jump involved (ultraviolet light has higher energy than visible light). Conversely, when light of the proper energy passes by the atom, the electron can jump in the reverse direction. Thus light is being continually absorbed and reemitted from atoms in the atmosphere. What often happens is that light may be absorbed from a beam (eg., from a target to a detector) and reemitted in another direction so that it is lost to the beam. As mentioned before, the energy of the light involved depends on the difference in energy levels in the atom. The energy (E) of the light is in turn related to the wavelength (λ) of the light by the relation $E = \frac{hc}{\lambda}$ and the frequency of the light (ν) by the relation $E = h\nu$ where h is Plank's constant and c is the velocity of light.

Atoms which are coupled to form molecules are not rigidly attached; they tend to vibrate about their center of mass in simple harmonic motion. As were the energy levels of the electrons within the atoms, the vibration energies are quantized. When a molecule goes from one vibration state to another, a quantum of energy is absorbed or given off. In like manner a molecule can rotate about its center of mass, and it has rotational energy states. The energy differences between rotational and vibrational energy states are much less than the energy difference between the electron shells so that the radiation absorbed is of longer wavelength. This radiation is called infrared radiation.

According to the Lambert-Beer Law, the decrease in spectral intensity of radiation by absorption with distance (x) is proportional to the intensity (I)

and the density (ρ) of absorbing molecules:

$$\frac{dI}{dx}(x,\nu) = - K(x,\nu) \; I(x,\nu) \; \rho(x) \; dx$$

where the proportionality constant (K) is called the absorption coefficient. This expression is then integrated to give the transmissivity (T), and assuming that K and ρ do not change significantly with distance:

$$T(\nu) = \frac{I(\nu)}{I_o(\nu)} = e^{-K(\nu)u}$$

where u is the mass of absorbing gas per unit area $u = \rho\Delta x$. In the absence of scattering the radiant absorptance (A) over a finite frequency interval ($\Delta\nu$) is then $A = \frac{1}{\Delta\nu} \int_{\Delta\nu} (1 - e^{-K(\nu)u}) \, d\nu$ since $A = 1 - T$.

Before evaluating $K(\nu)$ it should be noted that these energy transitions are not infinitesimal points on the frequency spectrum. The spectral lines have width. The two primary causes of line broadening in the atmosphere are due to the Doppler and the pressure effects. The observed frequency of a spectral line is changed by motion of the radiating molecule in the line of sight just as the time to move from one crest of a wave to the next on a lake is shortened when one is moving toward the source of the waves. This is called the Doppler effect. In the case of light, the frequency is decreased (or the color shifted from green to red) if the source is moving away from the observer. (This is the cause of the red-shift of distant galaxies moving rapidly away from the earth.) The molecules of a gas are constantly in motion in all directions so that some of them will appear to give off shorter wavelength radiation and others will give off longer wavelength radiation. This causes a spread in wavelengths. The higher the temperature (T), the faster the motion and therefore the greater the spread. The half-width at half maximum intensity of a Doppler broadened line is given by:

$$\Delta\nu_D = \frac{\nu_o}{c}\left(\frac{2kT}{m}\ \ln 2\right)^{1/2}$$

where ν_o is the center frequency, k is the Boltzmann constant and m is the mass of the molecule, (Wolfe, 1965).

In order for a molecule to emit a continuous wave train, it must be free from interruptions. However, atmospheric molecules undergo many collisions with other molecules in a short period of time and these collisions therefore cause a line broadening. This is called pressure, Lorentz, or collisional broadening, because it depends on pressure as well as temperature.

$$\Delta\nu_P = \Delta\nu_o \frac{P}{P_o}\left(\frac{T_o}{T}\right)^n$$

Here P_o and $\Delta\nu_o$ are evaluated at a reference temperature T_o. n depends on ν_o and the molecule involved (both the molecule that is radiating and the one with which it is colliding) but generally, $n \approx \frac{1}{2}$. P is not the total pressure because the absorbing molecules are more effective at broadening than the background molecules. For CO_2, P equals the total pressure plus 0.3 times the partial pressure of CO_2 (Anding, 1967). Occasionally for high concentrations of the absorbing gas, the effect due to absorbing molecules is separated from the effect due to background molecules and called self-broadening. If the partial pressure of the absorbing gas is small as is generally the case, it is a good approximation to use the total gas pressure. Burch et al., (1962) gives a good description of pressure broadening including self-broadening.

Pressure broadening is dominant at low altitudes in the earth's atmosphere and Doppler broadening is dominant at high altitudes. A general discussion of line broadening is given in Richtmyer et al., (1955).

Now that the half-widths of the spectral lines are known, the absorption coefficients can be written down. The absorption coefficient for pressure broadening for a frequency $\nu - \nu_o$ from the band center is:

$$K_p(\nu) = \frac{S}{\pi} \frac{\Delta\nu_p}{(\nu-\nu_o)^2 + (\Delta\nu_p)^2}$$

where S is the total line intensity. The absorption coefficient for Doppler broadening is:

$$K_D(\nu) = \frac{S}{\Delta\nu_D} \left(\frac{\ln 2}{\pi}\right)^{1/2} \exp\left[-\frac{\ln 2}{(\Delta\nu_D)^2} (\nu-\nu_o)^2\right].$$

If both Doppler and pressure broadening must be considered at once,

$$K(\nu) = \frac{(\ln 2)^{1/2}}{\pi^{3/2}} \frac{Sa}{\Delta\nu_D} \int_{-\infty}^{\infty} \frac{e^{-y^2}}{a^2 + (w-y)^2} dy$$

where $a = (\ln 2)^{1/2} \frac{\Delta\nu_P}{\Delta\nu_D}$, $w = (\ln 2)^{1/2} \frac{\nu-\nu_o}{\Delta\nu_D}$, $y = \frac{Su}{2\pi\Delta\nu_P}$.

u as previously mentioned is the mass of the absorbing gas per unit area. In principle it is now possible to find the absorptance of the gas. The problem is that all of this was done for only one line and each absorption band has many lines in it, many of which overlap each other. Also since the absorption coefficients depend on temperature, pressure, concentration of the absorbing specie as well as wavelength, the absorption coefficients will vary with altitude, geographical location, time of day, season, and local meteorological conditions. Therefore the absorptance must be calculated in layers after making many general assumptions and then the layers are added. This is generally done in a computer. Among others, McClatchey at AFCRL and Anding at the University of Michigan have computer programs to make these computations. Wolfe (1965) is a good general reference for the subject of atmospheric absorption. Anding (1967) goes into much greater detail.

Ozone in the upper atmosphere absorbs most of the ultraviolet light from the sun so that radiation with wavelengths shorter than 0.3μm is not useful to remote sensing. The visible spectrum is almost free of absorption except for a weak O_3 band between 0.5μm and 0.7μm. There are three narrow absorption

bands due to O_2 in the near infrared at 0.69μm, 0.76μm, and 1.25μm but most of the O_2 and N_2 absorption is in the far ultraviolet.

There are six gasses that are primarily responsible for molecular absorption of infrared radiation in the atmosphere: CO_2, N_2O, CO, CH_4, O_3, and H_2O (see figure 3). Carbon Dioxide is fairly uniformly mixed vertically throughout the atmosphere and averages about 320 ppm. Geographically CO_2 concentration can vary from 150 ppm in the polar regions to 700 ppm near Africa and in general is higher at night than during the day (Anding, 1967). CO_2 concentrations are also higher in industrial regions. The CO_2 content has been measured to be 10% higher downwind of London than when the wind was blowing the other way. A 10% increase in the average concentration of CO_2 has been noted between 1900 and 1950 (Glueckauf, 1951).

The measured concentration of Nitrous Oxide varies from 0.28 ppm to 1.25 ppm probably because the major sources of N_2O are the aerobic bacterial decomposition of nitrogen compounds and air pollution. The fractional concentration appears to be constant with altitude (Anding, 1967).

The concentrations of Carbon Monoxide and Methane also vary with location being higher near cities, but are uniformly mixed as a function of altitude. Typical values (not near a city) are 0.12 ppm for CO and 1.1 ppm for CH_4 (Anding, 1967).

Ozone varies greatly with altitude because it is formed primarily by photochemical dissociation of oxygen by ultraviolet radiation in the mesosphere (see Figure 4). Because of this distribution, O_3 absorption is much more important in satellite measurements than in airplane measurements. O_3 distribution varies with season and latitude (see Figures 5 and 6). The seasonal variation is roughly sinusoidal with a maximum in early spring and a minimum in the fall (Anding, 1967). The vertical profile of O_3 also changes with concentration and

season (see Figure 7). The relatively low-altitude maximum (12 km) that sometimes occurs in winter could be a problem with aircraft measurements. O_3 also increases during thunderstorms (Glueckauf, 1951).

Water vapor is probably the most important infrared absorber and it also has the greatest variation of concentration with location, altitude, and time. A typical H_2O sounding is given in Figure 8. If measurements are to be made which include an H_2O absorption band, the only accurate procedure is to monitor the water vapor, perhaps by using another wavelength channel to look at only the water vapor.

Wolfe (1965) gives absorption curves for the various absorption bands of CO_2, H_2O, N_2O, CO, and CH_4 at different equivalent pressures. He also describes methods for determining absorption along slant paths. An indication of the increased absorption for slant paths is given in Table 2. These equivalent air masses can be used both for determining the atmospheric absorption in the incident solar radiation and the radiation absorption of a ground target when the sensor is above the atmosphere on a satellite.

Figure 9 gives the results of high resolution measurements taken over fairly long paths at ground level (therefore Ozone is absent). Note the similarity of the curves for the various path lengths. Note also that the atmospheric "Windows" have many absorption lines within them.

In addition to the atmospheric gasses, aerosols are important in absorption of infrared radiation. Figure 10 shows the transmission of infrared radiation through quartz aerosols superimposed on CO_2 and H_2O absorption curves. These are theoretical curves taking into account both absorption and scattering, but the 8-9μm peak is primarily due to absorption. The size and mass distributions of the quartz particles are typical of a 1 km layer

centered at 850 mb over NW India. A density of 0.5 gm/kgm for H_2O and 0.24 cm/mb for CO_2 was assumed (Peterson, 1968).

Micas, clay minerals, quartz, and most other silicates absorb strongly around 10μm (see Table 3). This is the spectral region of the so-called atmospheric window. For this reason, one must be aware of aerosols as well as atmospheric gasses when using certain spectral intervals. More will be said about aerosols in the section on scattering.

4. Scattering

Pure scattering means only a redistribution of energy from its original direction of propagation with no attenuation. Numerous substances such as smoke will both scatter and absorb radiation, but the theoretical part of this section will be limited to pure scattering. When electromagnetic radiation falls upon an atom, the electrons in the atom begin to oscillate with the frequency of the radiation in the direction of the electric vector of the radiation. The accelerating electrons will then re-radiate in all directions perpendicular to the electric vector similar to an antenna. If the atoms are in a fixed lattice, destructive interference between the re-radiation from the various atoms will cancel virtually all except the forward radiation, and if not absorbed, the radiation will continue unimpeded except for a phase change related to the index of refraction.

The spacings between atoms of a gas, however, are irregular and continually changing. Therefore the radiation interference becomes negligible and re-radiation in other than the forward direction becomes possible. This type of scattering is called Rayleigh scattering. Rayleigh scattering applies when the radiation wavelength is much larger than the particle size. In the case of visible light, the radiation wavelength is several thousand times the size of individual atoms.

At right angles to the incident radiation, an interesting phenomenon occurs. Since radiation is not emitted in the direction of acceleration of the electron, only radiation with the electric vector perpendicular to the direction of scattering will appear. The scattered radiation is thus polarized even though the incident radiation is not. At angles other than right angles to the incident radiation, the scattered radiation will be only partially polarized.

In the atmosphere, however, even radiation scattered at 90° will not be completely polarized due to such effects as multiple scattering.

The transmissivity of a given path to radiation subjected to scattering is given by an expression similar to that for absorption:

$$T = e^{-\sigma x}$$

where x is the path length and σ is the scattering coefficient. For Rayleigh scattering:

$$\sigma = \frac{4\pi^2 N V^2}{\lambda^4} \quad \frac{(n^2-n_o^2)^2}{(n^2+2n_o^2)^2}$$

where N is the number of particles per unit volume, V is the volume of the scattering particle, n_o is the refractive index of the suspending medium and n is the refractive index of the scattering particles (Wolfe, 1965). Rayleigh scattering may also be expressed as:

$$\frac{I_s}{I_i} = \frac{8\pi^4 N \alpha^2 (1 + \cos^2\theta)}{\lambda^4 r^4}$$

where I_s is the intensity of scattered light, I_i is the intensity of the incident light, α is the particle polarizability, θ is the angle of scattering, and r is the distance from the scattering system to the point of observation (where $r >>$ any relevant dimension of the scattering system) (Hart, 1966).

The most important factor in the above equations is the fourth power dependence on wavelength. The shorter the wavelength, the greater the scattering. This means that blue light is scattered 5 to 10 times as much as red light. Since skylight is light from the sun scattered by the atmosphere, the sky appears blue. The sun, on the other hand, appears yellow because much of the blue has been removed. As the atmospheric path length is increased (ie., the sun is lower in the sky), the sun appears more red since more and more

short wavelengths are scattered out. At sunset, the atmospheric path is long enough for the red to be scattered, and since the blue has already been scattered out, the sky appears red. Rayleigh scattering contributes about 7% to the earth's albedo (Bartman, 1967).

The physical reason for the preferred blue scattering is that the restoring forces binding the electron in an atom give the electrons a natural frequency corresponding to the frequencies of violet or ultraviolet light. It is therefore easier to set up forced oscillations of the electrons if the incident radiation is of this frequency. The longer the wavelength, the more difficult this forcing becomes (Halliday et al., 1962).

As is indicated in the formula for the Rayleigh scattering coefficient, the intensity scattered is proportional to the number of scattering particles. This is true only if the atoms are far enough apart to be independent. Except for random density fluctuations, this is true for atmospheric gasses since the spacing is not small compared to the wavelength of light. However, if a number of atoms of the gas combine together to form a drop, such as happens when water vapor condenses, the atoms are spaced very closely compared to the wavelength of light and the atoms are no longer independent. Since the atoms are acting together, the electric field will be multiplied by the number of atoms. This means that the intensity scattered will be multiplied by the number of atoms squared (Feynman, 1963). This is why clouds scatter much more than the sky. The increase in scattering with the square of the number of particles will not continue indefinitely. When the water droplet is too big, the atoms on one side of the droplet become independent of those on the other side. Due to its shorter wavelength, blue light reaches this limit before red light. Although the blue light scatters more per atom than red

light, there is a bigger enhancement for red light when most of the drops are bigger than the wavelength; hence for large drops, there is little wavelength dependence. Since cloud drops are bigger than visible wavelengths, (see Figure 11), clouds appear white rather than blue. For derivations and further discussions of Rayleigh scattering including polarization effects and angular dependences, see Condon, 1958 and Born, 1965. Coulson et al., (1960) have tables of Rayleigh scattering.

Rayleigh scattering is a good scattering theory only for particles of diameter less than about one-tenth the wavelength of the incident light (Condon, 1958). For aerosol particles of the same order of magnitude as the incident wavelength, Mie theory must be used where:

$$\sigma = \pi \int_{a_1}^{a_2} N(a)\ K(a,n)\ a^2 da$$

$N(a)$ is the number of particles per unit volume in the interval da and $K(a,n)$, which depends on both the particle radius (a) and the particle index of refraction (n), is the scattering area coefficient. The particle size distribution extends from a_1 to a_2 (Wolfe, 1965). For water droplets, $K(a,n)$ has the form shown in Figure 12. Table 4 gives further values of K for various n and α (defined as circumference of the particle divvided by the wavelength of the radiation).

It should be noted that as was hinted earlier, there is little wavelength dependence in this scattering coefficient. For this reason a dusty or polluted sky appears gray rather than blue. Other results of Mie theory, of which Rayleigh scattering is a limiting case, are a depolarization of light scattered through 90° and a dissymmetry that makes forward scattering more intense than backward scattering (Condon, 1958). An example of this strong forward scattering is the bright aureole surrounding the sun (Bartman, 1967).

In general, for a fixed mass per unit volume, scattering is a maximum when the particle size is of the order of the incident radiation wavelength and diminishes for both smaller and larger particles (Condon, 1958). A thorough discussion of Mie theory is given in Van de Hulst (1957). A good description of Mie theory including tables of Mie scattering is given in Deirmendjian (1969).

Nonselective scattering occurs when the scattering particles are large compared to the incident radiation wavelength. This process is a combination of surface reflection, transmission, and edge diffraction. Combining these effects and including the interference between them gives the result that for particles with diameters greater than about six wavelengths, the scattering area coefficient (K) is about two. This agrees with Mie theory (Wolfe, 1965). A more detailed description of nonselective scattering is given in Kruse (1962).

Mie theory applies only to spherical particles. Water drops are generally spherical but dust and ash particles are irregular in shape. For irregular particles, it is a good approximation to use spherical particles with the same surface area in the theory. This approximation, however, will not predict polarization or large angle scattering properly (Anding, 1970).

Real atmospheric scattering is next to impossible to calculate. A complete solution would need to contain multiple scattering, both molecular and aerosol, aerosol particle size distributions as a function of altitude, atmospheric absorption, and surfaces such as clouds or the ground which may reflect radiation into the path under consideration, all as a function of wavelength and sun angle (Bartman, 1967).

It would be nice to have an empirical expression for scattering, perhaps similar to the Rayleigh scattering law but with another exponent. Kruse (1962) derives the following expression for the transmitted intensity in the ith wavelength interval as affected by scattering:

$$T_{si} = \exp\left[-\frac{3.91}{V}\left(\frac{\lambda_i}{0.55}\right)^{-q}x\right]$$

Where x is the path length, λ_i is the wavelength in micrometers, and V is the meteorological range defined as the distance at which the average eye can just barely detect a large, black object against the horizon sky. More will be said about the meteorological range in the section on contrast. On days when seeing conditions are very good, $q = 1.6$; on days of average seeing conditions, $q = 1.3$; and when the meteorological range is less than 6 km, $q = 0.585\ V^{1/3}$. Quenzel (1970) gives examples of measured extinction coefficients vs. wavelength.

Since the mass and size distribution of aerosol particles plays such an important role in scattering, some experimental results will now be given. Figure 13 shows the size distribution of natural aerosol particles in continental air and Figure 14 the same for maritime air (sea salt) at about 80% relative humidity and various wind speeds. N is the total number of particles per cm^3 with radii (in μm) from the lower limit up to R. Figure 15 gives the typical vertical profiles of aerosols where N is the number concentration per cm^3 of the size particles plotted. The giant particles refer to sea salt and profiles are given both for over the source area and continents. Aitken particles are less than 0.1μm and large particles range between 0.1μm and 1μm. Figure 16 gives the vertical profile of aerosol number density for a clear standard atmosphere, and Figure 17 gives a vertical profile for an extreme case of aerosol concentration, namely over the NW Indian desert. [Peterson (1968) found that scattering from these particles does not follow Mie theory.] There is a concentration of dust near the mesopause (see Figure 1) probably due to meteorite activity. When noctilucent clouds are present, at these high altitudes, the dust concentration is 10^3 times greater at this altitude (84 ± 4 km)

than when absent (see Figure 18). The particles are primarily iron, nickel, and silicon (Erickson, 1969). The clouds scatter sunlight according to Mie theory. The scattered light is eliptically polarized ranging from 5% at 20° scattering angle to 50% at 60° scattering angle (Valley, 1965). Table 5 gives the concentration (in gm/m^3) of aerosols for different air mass conditions. It gives an indication of horizontal variations and points out the importance of pollution aerosols. Table 6 gives the increase in aerosol concentration under extreme conditions.

To show how variable the atmosphere can be, Figure 19 gives the variation of scattering coefficients with height on various occasions of "clean air". Figure 20 does the same for industrial haze.

In summary, it should be stated that in general both absorption and scattering should be considered. Möller (1964) claims that scattering of terrestrial radiation (infrared) by gasses or aerosols (even clouds) is an insignificant part of the extinction compared to absorption. This is due to the large absorption and long wavelengths. On the other hand the visible spectrum is almost free of absorption. In most aerosols, the index of refraction changes widely with wavelength (Peterson, 1968); however, the size distribution is continuous, therefore scattering is a much smoother function of wavelength than absorption.

5. Index of Refraction Changes

Besides being absorbed and scattered, electromagnetic radiation can be bent or refracted by the atmosphere in the same way light is refracted in a lens. The index of refraction of the gaseous atmosphere (n) depends on pressure (p in mmHg), temperature (t in °C), vapor pressure (f in mmHg), and wavelength (λ in μm):

$$n=1+\frac{(272.7+1.482\lambda^{-2}+0.020\lambda^{-4})p[1+(1.049-0.0157t)10^{-6}p]-(46.136512-0.49020044\lambda^{-2})f}{720.883(1+0.003661t)}$$

(Kingslake, 1965). A much simpler expression for index of refraction for dry air is given by Wark et al., (1964):

$$n = 1 + C\frac{p}{t} \quad , \quad C = 77.526 \times 10^{-6} \quad \frac{^{\circ}k}{mb}$$

Figure 21 is a nomograph for computing the refractive modulus (N) of dry air at optical wavelengths.

$$N = 10^{6} (n - 1)$$

This nomograph is good to within about 5 units of N. In general, the index of refraction decreases with altitude so that radiation entering the atmosphere at any angle follows a curved path. For example, the apparent position of stars near the horizon is about 0.5° higher than the true position (see Figure 22). This increases the path length of the radiation. In the vicinity of a cold body of water, the air density (and thus the index of refraction) can decrease much more rapidly with altitude than normal and a phenomenon called "looming" can occur. Light rays are bent downward so that looking up one can see an object which is on the water surface appear to be floating in mid-air (see Figure 23). When the earth's surface is very hot the air near the surface becomes much warmer than at higher altitudes and the lapse rate (temperature vs. altitude) is much steeper than normal. In this condition of unstable equilibrium

the air density actually increases with height near the surface; therefore, the light rays are bent upward. An object appears to be reflected in the surface as though there were water present (see Figure 24). This phenomenon is called a mirage. These phenomena are discussed by Rossi (1957).

More serious optical effects occur due to rapid irregular changes in the index of refraction over distances of 3-8 inches and times of 0.05 sec (Kingslake, 1965). These effects go by various names: scintillation, atmospheric boil, image jitter, optical haze, twinkling, or shimmer. Since convection currents are among the main contributors to these fluctuations, scintillation is most evident on sunny days; however, twinkling stars are a prime example of this phenomenon. The image displacement amounts to only 15 to 30 seconds of arc under severe ground to ground conditions (Wolfe, 1965), but the problem is that there is little correlation between the instantaneous deviations of any two points separated by 5 minutes of arc or more (Middleton, 1952). Thus there can be great distortion of small objects. This effect, however, is less noticed in extended objects which is why planets do not twinkle. This time varying image distortion causes loss of fine detail and limits obtainable resolution. A typical diurnal cycle of scintillation over a grass surface is given in Figure 25.

The illumination as well as the apparent direction of an object can be affected (Middleton, 1952). Another effect of scintillation is image enlargement. The atmosphere acting like a time varying lens will defocus the image. No matter whether the new focal point is behind or in front of the old one, a point in the original focal plane will be spread out. For further discussion on scintillation, including wind speed dependence, see Wolfe (1965).

A note about making measurements, especially from airplanes, should be made at this point. The index of refraction of the atmosphere can be changed

by pressure changes due to air flow around the airplane or camera housing, sound pressure waves from engines, gas type variations, and aerosols in addition to the parameters mentioned at the beginning of this section.

One last point is that image degradation of ground resolution due to scintillation for a given atmospheric condition will become less and less noticeable with increasing altitude while the geometrical ground resolution falls off with altitude (Polcyn, 1967).

6. Natural Solar and Infrared Radiation

Most radiating objects are given in terms of a blackbody temperature. In reality this is difficult because there are many different processes going on. Even outside the earth's atmosphere, the solar spectral irradiance cannot be characterized by any single blackbody temperature. It is 4500°K at 0.2μm wavelength, 5900°K in the yellow green at 0.56μm, 5600°K at 4.0μm, 5300°K at 5.0μm, and 5040°K at 11.1μm. In the microwave region the radiance temperature of the solar corona reaches 1 to 2 X 10^6 °K (Valley, 1965). Superimposed on this complex blackbody curve are numerous absorption bands due to the solar atmosphere. Figure 26 gives the solar irradiation both outside the earth's atmosphere and at sea level compared to a 5900°K blackbody curve. Gates (1966) describes the spectral Distribution of Solar Radiation at the earth's surface.

The natural illumination of objects depends on how the atmosphere has altered the radiation of the sun by absorption and scattering. Figures 27 and 28 show the transmission of the atmosphere for different sun zenith angles. The sun zenith angle in turn is a function of latitude, time of day, and time of year. Figure 29 compares solar altitude with illuminance for average clear weather. For a rough approximation, divide the values by two for thin clouds and by three for average clouds. Figure 30 shows the illumination for different dates and latitudes for local noon, and Figure 31 shows the same for local noon ± 4 hours. Harvey et al., (1965) shows similar figures for other times of the day.

The natural light which illuminates most terrestrial objects is a combination of sunlight and skylight. The sunlight ranges roughly between a 5600°K and a 5800°K blackbody radiator depending on the solar zenith angle. (As men-

tioned earlier, Rayleigh scattering shifts the sunlight toward the red end of the spectrum which means a lower blackbody temperature). On the other hand, the predominancy of blue makes skylight range from 10,000°K to 60,000°K depending on sun angle and weather conditions (Harvey et al., 1965). An object in the sun is illuminated by both sunlight and skylight which average to about 6,000°K. However, objects in the shade will be illuminated by much bluer light (see Figure 32).

Bidirectional reflectance (ρ') is the fraction of radiation incident from the direction (θ_i, ϕ_i) which is reflected in the direction (θ_r, ϕ_r). Here θ_i and θ_r are zenith angles and ϕ_i and ϕ_r are azimuth angles (see Figure 33). The radiance N_r in the direction (θ_r, ϕ_r) is then:

$$N_r(\theta_r, \phi_r) = \int_h \rho'(\theta_i, \phi_i, \theta_r, \phi_r)\, N_i(\theta_i, \phi_i) \cos\theta_i \, d\Omega_i$$

where N_i is the source radiance which subtends a solid angle $d\Omega_i = \sin\theta_i d\theta_i d\phi_i$ at A_s. h indicates integration over a hemisphere (Nicodemus, 1965).

The directional reflectance (ρ_d) is defined as the ratio of radiation incident A_s from the direction (θ_i, ϕ_i) to that reflected in all directions. It is related to the bidirectional reflectance by:

$$\rho_d(\theta_i, \phi_i) = \int_h \rho'(\theta_i, \phi_i, \theta_r, \phi_r) \cos\theta_r d\Omega_r$$

(Nicodemus, 1965). For perfectly diffuse (Lambertian) reflectance,

$$\rho_d = \pi\rho' = \text{constant}$$

Neglecting skylight and assuming that ρ' and N_i are constant over $\Omega_\odot$ which is the solid angle subtended by the sun, the bidirectional reflectance becomes:

$$\rho'(\theta_i, \phi_i, \theta_r, \phi_r) = \frac{N_r(\theta_r, \phi_r)}{N_\odot(\theta_i, \phi_i)\, \Omega_\odot \cos\theta_i}$$

where $N_\odot$ is the sun's radiance and θ_i and ϕ_i are now the zenith and azimuth of the sun. For a Lambertian surface:

$$\rho_d = \frac{\pi N_r}{N_\odot (\theta_i, \phi_i) \Omega_\odot \cos \theta_i}$$

(Peekna, et al., 1970).

Since most surfaces are not Lambertian, an anisotropy factor (χ) may be defined as:

$$\chi (\theta_i, \phi_i, \theta_r, \phi_r) = \frac{\rho_d(\theta_i, \phi_i)}{\pi \rho'(\theta_i, \phi_i, \theta_r, \phi_r)}$$

(Brennan et al., 1970). For Lambertian surfaces $\chi = 1$. Table 7 gives anisotropy factors for various surfaces and atmospheres. Figure 34 shows reflected radiance vs. wavelength for snow fields.

The radiant power incident on an object is the product of the source radiance, the solid angle subtended by the source, and the object area. The radiance of the sun is independent of the distance from the sun, but the solid angle subtended by the sun decreases as the square of the distance from the sun (at large distances). For this reason the radiant power from the sun incident on an object is less important than atmospheric emission (large solid angle) for wavelengths greater than about 4μm even though the radiance from the sun (watts $\cdot$ m^{-2} $\cdot$ $ster^{-1}$) is greater than the radiance from the atmosphere at these wavelengths (see Figure 35).

The atmosphere emits like a graybody radiator (a blackbody radiator with emissivity less than one) having the temperature of the atmosphere at that point (200°K to 300°K). Figure 36 gives the infrared spectral radiance of a clear zenith sky as a function of sun angle. The atmospheric emission does not change much with sun angle; however, the scattered sunlight changes quite a bit. Figure 37 gives the spectral radiance of a sky covered with cirrus clouds at various look angles. The ground also emits like a graybody. Whether

an observer sees the ground or the atmosphere depends on the opacity of the atmosphere at that wavelength. An example of radiation reaching a satellite is given in Figure 38. The infrared interferometer spectrometer on Nimbus III was used, and the effect of major absorbing bands of atmospheric gasses is evident.

As mentioned earlier, skylight is partly polarized due to Rayleigh scattering. The polarization is strongest where the sky is darkest at about 90° from the sun.

Figure 39 gives the atmospheric luminance vs. solar altitude for clear weather conditions using a minus blue filter. The decrease above 25° indicates less scattering in the shorter path length. The decrease below 25° is due to attenuation of the sun's rays (Harvey et al., 1965).

7. Contrast

The contrast (c) between two objects of radiance N and N' (or object N and background N') is defined in at least three ways in the literature:

$$C_1 = \frac{N-N'}{N'} \quad , \quad C_2 = \frac{N-N'}{N+N'} \quad , \quad \text{and} \quad C_3 = \frac{N}{N'}$$

The first definition is used by Duntley (1948) and Middleton (1952) and will be used in this paper unless otherwise noted. The inherent contrast (C_o) is the actual contrast as viewed at the object and the apparent contrast (C_R) is the contrast as viewed from a distance R. Inherent radiance (N_o) and apparent radiance (N_R) are similarly defined.

Two things can happen to a beam of light between the object and the detector. First, the light within the beam can be absorbed or scattered out of the beam, and second, light from outside the beam can be scattered into the beam and the atmosphere can emit radiation into the beam. Both of these phenomena depend on the path length.

As an example, suppose $N_o = 3$ and $N_o' = 1$. This gives an inherent contrast of 2. Now suppose the atmosphere adds 1 unit to both N_o and N_o', then $C_R = \frac{4-2}{2} = 1$, a reduction of contrast. If in addition both N_o and N_o' are reduced by 0.5 by the atmosphere, then $C_R = \frac{[(3)(.5) + 1] - [(1)(.5) + 1]}{[(1)(.5) + 1]} = \frac{2}{3}$, a further reduction in contrast. Thus a dark mountain against a light sky will appear to get lighter with distance until the mountain and sky are the same brightness making the mountain invisible. In like manner a sunlit, snow-clad mountain against a darker background will appear darker as viewed from further and further away until it, too, disappears against the background.

Following Duntley (1948), this can be put mathematically as follows:

$$N_R = \frac{\sigma_o W}{\beta_o} (1 - e^{-\beta_o \bar{R}}) + N_o e^{-\beta_o \bar{R}}.$$

where σ_o is the scattering rate coefficient at the object, W is the spectral radiant density of the atmospheric light, β_o is the atmospheric attenuation coefficient near the object and $\bar{R}$ is the optical slant range. Physically, the optical slant range is the horizontal distance in a homogeneous atmosphere for which the attenuation is the same as that along the path to R. If the above expression for N_R (and a similar one for N_R') is put into the equation for apparent contrast, the law of contrast reduction by the atmosphere is found:

$$C_R = \frac{N_R - N_R'}{N_R} = \frac{N_o'}{N_R'} C_o e^{-\beta_o \bar{R}}$$

Assuming that $N_o' = N_R'$, then $C_R = C_o T_R$ where $T_R = e^{-\beta_o \bar{R}}$ is the contrast transmittance.

Previously the meteorological range (V) was defined as the distance at which the average eye can just barely detect a large, black object against the horizon sky. Since this original definition was subjective, meteorological range is now defined as that horizontal distance for which the contrast transmittance (T_R) is two percent. Hence, $V = \frac{3.912}{\beta_o}$. Since in practice, the meteorological range is still found by the old method and observable black objects are rarely large enough so that increasing the size would not change the contrast, the reported "visibility" is usually less than the meteorological range. A study showed that on the average the "visibility" was three-fourths the meteorological range (Duntley, 1948).

The optical slant range can be found from the meteorological range and the inherent contrast under full daylight conditions using the nomogram in Figure 40. A point is noted at the right edge on a straight line connecting

the sky-ground ratio with the inherent contrast. This point is then connected by a straight line with the meteorological range. Where this second line crosses the proper target area, the value of $\overline{R}$ can be observed (Middleton, 1952).

It should be noted here that it has been shown by photographing resolving power targets that haze, although reducing contrast, does not obliterate details (Duntley, 1948). On the other hand, more detail will be obliterated on a clear day due to atmospheric scintillation.

A telescope can increase the range at which an object can be seen by increasing the angle the object subtends. A telescope cannot, however, increase the contrast. In fact, the telescope optics will act like additional atmosphere and reduce the contrast further (Middleton, 1952).

A computer program which simulates contrast reduction has been developed by Breitling et al., (1970). (The contrast definition used is that given by C_2 at the beginning of this section.) Some of the results of this program will now be given. Figure 41 gives the spectral variation of the apparent contrast for four atmospheres of varying turbidity. The Rayleigh atmosphere has no aerosols; the Elterman model has a sea level visibility of about 25 km; the typical model has a visibility of about 12 km; and the dirty model has a visibility of only 3 km. It should be noted that the dirty model has lost almost all wavelength dependence, because Rayleigh scattering is small compared to Mie scattering. The discontinuity in the curves beyond 0.75μm is caused by the high reflection of the vegetation background. This reduces the apparent contrast by increasing the atmospheric path radiance. Figure 42 gives the contrast reduction dependence on solar zenith angle and Figure 43 the dependence on nadir look angle.

An example of experimental results is given in Figure 44 (the contrast definition is that given by C_2). The contrast reduction vs. altitude was measured photographically using several filters. The airplane flew over large (48 foot square) black and white panels having reflectances of 0.05 and 0.9 respectively (Majarowski, 1965).

8. Spectral Signature

Various atmospheric phenomena can have an effect on the spectral signature of an object. As mentioned in the section on natural illumination, the radiation impinging on an object can change with time. Figure 45 shows the spectral distribution of incident solar radiation at various times during the day. Not only the intensity of the light is different, some of the peaks have changed wavelength. The fact that the infrared to visible radiation ratio is lower in the morning than in the afternoon is probably due to the increase of aerosols which often occurs during the day (Yost, 1969).

Two things can happen to the beam of light once it has been reflected off the object of interest. First, attenuation and scattering can preferentially decrease the intensity of one wavelength more than another, and second, the light scattered into the beam may be of a different color. The latter can be thought of as the mixture of the object color and the air-light color. Middleton (1952) discusses the theory of mixing colors, but here only experimental results will be given. It should be clear, however, that more color mixing will appear on a clear day than on a hazy day, because a Rayleigh sky is blue and a Mie sky is white.

Figure 46 shows the color shift with altitude of four target panels. The blue and green targets have considerable ambiguity as the altitude is increased since the colors overlap. Figure 47 shows the spectral signatures of high and low chlorophyll seawater at various altitudes. The high chlorophyll concentration was about 0.22 mg/m^3 with a mean temperature of 18°C, and the low chlorophyll concentration was about 0.07 mg/m^3 with a mean temperature of 25°C. The The look angle was 40° incidence, pointed away from the sun's glitter pattern. The sun's zenith angle was less than 48° and empirical corrections for the

angle were applied to the spectra. The atmosphere was clear and the sea state was low (Clarke et al., 1969). Since the nonspecular reflectance of water is low, the addition to the light beam is more significant than the depletion of the light beam from the target; therefore, the radiance increases with altitude, the difference between the high-chlorophyll and low-chlorophyll spectra decreases with altitude, however. Middleton (1952) noticed an effect of industrial haze. A bluish-white mercury vapor lamp appeared green at 100 m and yellow at 200 m.

A more subtle effect is the change of spectra with decreasing viewing angle. Figure 48 shows a chromaticity diagram deformed to give roughly equal spacing to colors equally different in appearance. Twenty such colors are plotted as open circles. The solid dots show the apparent locations of the colors when observed as spots subtending two minutes of arc on a gray background. Red and blue-green are not changed much but yellow-green and purple become almost gray. This effect appears with subtending angles of about 15 minutes or less (Middleton, 1952).

One final note is that whereas color differences can help identification since there are both luminosity and chromaticity contrasts, at large distances color may not help. This is because any color is likely to appear achromatic with the addition of air light by the time its luminosity contrast has gone to zero (Middleton, 1952). In addition to this, distant objects subtend very small angles and the angular effect just mentioned becomes important.

9. Concluding Remarks

A generalized theory to cover the various atmospheric effects on remote sensing is not available because of the many variables involved including temperature, pressure, moisture, cloud cover, wind, aerosol concentration, aerosol size distribution, aerosol composition, ozone concentration, sun angle, look angle, ground surface reflection properties, convection currents and lapse rate, all of which may change in time and space, both horizontally and with altitude. Even an empirical theory is difficult, because the same variables are involved. The only approach is then to minimize the significance of these variables for the particular experiment involved and monitor the ones which may give trouble. The experimental results can then be interpreted with this information in mind.

Acknowledgements

We thank the members of the Wisconsin Remote Sensing Project for their encouragement, especially Professor James Clapp. The study was supported by NASA.

Dr. Thomas VonderHaar, principal investigator, is presently affiliated with the Department of Atmospheric Science, Colorado State University.

References

Anding, Daivd, Band Model Methods for Computing Atmospheric Slant-Path Molecular Absorption, Report No. 7142-21-T. Willow Run Laboratories, The University of Michigan, Ann Arbor, 1967.

Anding, Daivd, Lecture in Advanced Infrared Technology Short Course at the University of Michigan, 1970.

Bartman, Fred L., The Reflectance and Scattering of Solar Radiation by the Earth, University of Michigan Technical Report 05863-11-T, 1967.

Born, Max, and Emil Wolf, Principles of Optics 3rd Ed., Pergamon Press, New York, 1965.

Breitling, P.J. and S. Pilipowskyj, "Computer Simulation of Optical Contrast Reduction Caused by Atmospheric Aerosol", AIAA Paper No. 70-194, AIAA 8th Aerospace Sciences Meeting, New York, 1970.

Brennan, B. and W.R. Bandeen, "Anisotropic Reflectance Characteristics of Natural Surfaces", Appl. Opt. 9, 405-412, 1970.

Burch, D.E., D. Williams, D. Gryvnak, E.B. Singleton and W.L. France, Infrared Absorption by Carbon Dioxide, Water Vapor, and Minor Atmospheric Constituents, Ohio State University Research Report, AD 287 406, 1962.

Clarke, George L., Gifford C. Ewing and Carl J. Lorenzen, "Remote Measurement of Ocean Color as an Index of Biological Productivity", Proceedings of the Sixth International Symposium on Remote Sensing of Environment, Vol. II, 991-1001, 1969.

Condon, E.V., "Electromagnetic Waves" in Handbook of Physics Ed. by E.V. Condon and High Odishaw, McGraw-Hill, New York, 1958.

Coulson, Kinsell L., Jitendra V. Dave and Zdenek Sekera, Tables Related to Radiation Emerging from a Planetary Atmosphere with Rayleigh Scattering, University of California Press, Berkeley, 1960.

Deirmendjian, D., Electromagnetic Scattering on Spherical Polydispersions, Am. Elsevier, New York, 1969.

Duntley, Seibert Q., "Reduction of Apparent Contrast by the Atmosphere", J. Opt. Soc. Am. 38, 179-190, 1948.

Erickson, Jon D., "A Review of Active Remote Sensing of the Atmosphere with Ground-Based Laser Radar", Proceedings of the Sixth International Symposium on Remote Sensing of Environment, Vol. I, 275-295, 1969.

Feynman, Richard P., Robert B. Leighton, and Mathew Sands, The Feynman Lectures on Physics, Vol. I, Addison-Wesley, Reading, Mass., 1963.

Gates, David M., "Spectral Distribution of Solar Radiation at the Earth's Surface", Science, 151, 523-529, 1966.

Glueckauf, E., "The Composition of Atmospheric Air" in Compendium of Meteorology, Ed. by Thomas F. Malone, American Meteorological Society, Boston, 1951.

Hanel, R., Goddard Space Flight Center, NASA, private communication, 1970.

Hart, R. W., "Light Scattering" in Encyclopedia of Physics, Ed. by Robert M. Besançon, Reinhold, New York, 1966.

Harvey, D. I. and E. P. Myskowski, "Physics of High Altitude Photography", in Photographic Considerations of Aerospace, Ed. by H. J. Hall and H. K. Howell, Itek Corp., Lexington, Mass., 1965.

Holliday, David and Robert Resnick, Physics for Students of Science and Engineering, Part II, 2nd Ed., John Wiley & Sons, New York, 1962.

Hovis, Warren A., Goddard Space Flight Center, NASA, private communication, 1969.

Hunt, John M., Mary P. Wisherd and Lawrence C. Bonham, "Infrared Absorption Spectra of Minerals and Other Inorganic Compounds", Anal. Chem., 22, 1478-1497, 1950.

Kingslake, Rudolf, Ed., Applied Optics and Optical Engineering, Vol. I, Academic Press, New York, 1965.

Kruse, Paul W., Laurence D. McGlauchlin, and Richmond B McQuistan, Elements of Infrared Technology: Generation, Transmission, and Detection, John Wiley & Sons, New York, 1962.

Mazurowski, Melvin J. and D. Roger Sink, "Attenuation of Photographic Contrast by the Atmosphere", J. Opt. Soc. Am. 55, 26-30, 1965.

Middleton, W. E. Knowles, Vision Through the Atmosphere, University of Toronto Press, 1952.

Möller, F., "Optics of the Lower Atmosphere", Appl. Opt. 3, 157-166, 1964.

Nicodemus, Fred E., "Directional Reflectance and Emissivity of an Opaque Surface", Appl. Opt. 4, 767-773, 1965.

Nicodemus, Fred E., "Radiance", Am. Jour. Phys. 31, 368-377, 1963.

Peekna, Susan K., Robert J. Parent and Thomas H. VonderHaar, "Possibilities for Quantitative Radiance Measurements in the 450-650 nm Region from the ATS-I Satellite", Annual Report on Contract NAS 5-11542, 1970 in Press. Available from Space Science and Engineering Center, 1225 West Dayton Street, Madison, Wisconsin 53706.

Peterson, James Teigen, Measurement of Atmospheric Aerosols and Infrared Radiation Over Northwest India and their Relationship, Ph.D. Thesis, Department of Meteorology, University of Wisconsin, 1968.

Polcyn, Fabian C., Investigation of Spectrum-Matching Sensing in Agriculture, Semi-annual Report No. 6590-9F(1), University of Michigan, Willow Run Laboratories, 1967.

Quenzel, H., "Determination of Size Distribution of Atmospheric Aerosol Particles from Spectral Solar Radiation Measurements", J. Geophys. Res. 75, 2915-2921, 1970.

Richtmyer, F. K., E. H. Kennard, and T. Lauritsen, Introduction to Modern Physics, 5th Ed., McGraw-Hill, New York, 1955.

Rossi, Bruno, Optics, Addison-Wesley, Reading, Mass., 1957.

U. S. Standard Atmosphere, 1962, NASA, USAF, U. S. Weather Bureau, For sale by U. S. Government Printing Office, 1962.

Valley, Shea L., Ed., Handbook of Geophysics and Space Environments, McGraw-Hill, New York, 1965.

Van de Hulst, Hendrik C., Light Scattering by Small Particles, John Wiley & Sons, New York, 1957.

Wark, D. Q., J. Alishouse, and G. Yamamoto, "Variation of the Infrared Spectral Radiance near the Limb of the Earth", Appl. Opt. 3, 221-227, 1964.

Wolfe, William L., Handbook of Military Infrared Technology, Office of Naval Research, For sale by U. S. Government Printing Office, 1965.

Yost, Edward and Sondra Wenderoth, "Agricultural and Oceanographic Application of Multispectral Color Photography", Proceedings of the Sixth International Symposium on Remote Sensing of Environment, Vol. I., 145-173, 1969.

Figure Legends

Figure 1: Temperature-height profiles of U. S. Standard Atmosphere, 1962, compared to those of Air Research & Development Command Model Atmosphere, 1956 and 1959 (Valley, 1965).

Figure 2: Vertical distribution of atmospheric constituents (Kingslake, 1965).

Figure 3: Comparison of the near-infrared solar spectrum with spectra of various atmospheric gasses (Valley, 1965).

Figure 4: Typical ozone concentration profile. Solid curve developed from ozonesonde network data, dashed curve from chemical equilibrium theory (Valley, 1965).

Figure 5: Average distribution of total ozone over the Northern Hemisphere in the spring. Multiply numbers given on contours by 10^{-3} to obtain values in atm-cm (Valley, 1965).

Figure 6: Average distribution of total ozone over the Northern Hemisphere in the fall. Multiply numbers given on contours by 10^{-3} to obtain values in atm-cm (Valley, 1965).

Figure 7: Mean seasonal distribution of ozone at about 52°N (Wolfe, 1965).

Figure 8: Typical variation of atmospheric water vapor with altitude (Anding, 1967).

Figure 9: Sea level atmospheric transmission (Kruse, 1962).

Figure 10: Theoretical transmission through a 1 km thick atmospheric layer as a function of wavelength resulting from the presence of quartz aerosols, water vapor, and carbon dioxide. The aerosol size distribution is proportional to r^{-4} (Peterson, 1968).

Figure 11: Typical drop-size distributions for a coastal fog and a cloud (Middleton, 1952).

Figure 12: Scattering area coefficient vs. size parameter for spherical water droplets (n = 1.33) of radius a (Wolfe, 1965).

Figure 13: Aerosol size distribution in continental air (Valley, 1965).

Figure 14: Aerosol size distribution in maritime air (Valley, 1965).

Figure 15: Vertical profile of the number concentration N (cm^{-3}) for various size particles (Valley, 1965).

Figure 16: Aerosol number density vs. altitude for a clear standard atmosphere (Valley, 1965).

Figure 35: Spectral radiance of a blackbody at the temperature in °K shown on each curve. The diagonal line indicates the wavelength of maximum radiance. Subdivisions of the ordinate scale are at 2 and 5 (Valley, 1965).

Figure 36: Spectral radiance of a clear zenith sky as a function of sun position (Wolfe, 1965).

Figure 37: The spectral radiance of sky covered with cirrus clouds at several "look" angles (Wolfe, 1965).

Figure 38: Radiance vs. wavelength taken from the infrared interferometer spectrometer on Nimbus III (Hanel, 1970).

Figure 39: Atmospheric luminance vs. solar altitude for clear weather conditions (Harvey et al., 1965).

Figure 40: Nomogram for determining optical slant range ($\overline{R}$) in full daylight using a detection probability of 95 per cent. See text for explanation (Middleton, 1952).

Figure 41: Spectral variation of apparent contrast. Inherent contrast is 0.5. The sun zenith angle is 60° and the look angle is straight down from the top of the atmosphere (Breitling et al., 1970).

Figure 42: Solar zenith angle dependence on apparent contrast. Inherent contrast is 0.5, the wavelength is 0.55μm, and the look angle is straight down from the top of the atmosphere (Breitling et al., 1970).

Figure 43: Nadir look angle dependence on apparent contrast for typical turbidity (see text) and various solar zenith angles. Inherent contrast is 0.5 and wavelength is 0.55μm. The detector is at the top of the atmosphere looking in the detector-sun-target plane which is perpendicular to the surface (Breitling et al., 1970).

Figure 44: Apparent white-black contrast vs. altitude using various filters. o aircraft ascent; ● aircraft descent (Mazurowski), 1965).

Figure 45: Spectral distribution of incident solar radiation on flat ground at various times of the day (Yost, 1969).

Figure 46: Chromaticity plot of the colors of target panel images on aerial ektachrome film as a function of altitude on a relatively clear day. The dots represent the altitudes in increasing order: 1500, 3000, 5000, 10000, 15000 and 28000 feet (Yost, 1969).

Figure 47: Spectra of sunlight backscattered from chlorophyll-rich and chlorophyll-poor seawater at various altitudes (Clarke et al., 1969).

Figure 48: The effect of small subtense on various colors (Middleton, 1952).

Table 1 Radiometric quantities, symbols, definitions and units (Nicodemus, 1963)

Quantity	Symbol	Defining relations	Units
Radiant energy	U		J
Radiant energy density	u	$u \equiv \frac{\partial U}{\partial V}$	$J \cdot cm^{-3}$
Radiant power	P	$P \equiv \frac{\partial U}{\partial t}$	watt (W)
Radiant intensity	J	$J \equiv \frac{\partial P}{\partial \Omega}$	$W \cdot sr^{-1}$
Radiant emittance	W	$W \left. \right\} \equiv \frac{\partial P}{\partial A}$	$W \cdot cm^{-2}$
Irradiance	H	$H \left. \right\}$	
Radiance	N	$N \equiv \frac{\partial^2 P}{\cos\theta \partial A \partial \Omega}$	$W \cdot cm^{-2} \cdot sr^{-1}$
Wavelength	λ		micron (μ)
Spectral radiant power	P_λ	$P_\lambda \equiv \frac{\partial P}{\partial \lambda}$	$W \cdot \mu^{-1}$
Spectral radiant intensity	J_λ	$J_\lambda \equiv \frac{\partial J}{\partial \lambda}$	$W \cdot sr^{-1} \cdot \mu^{-1}$
Spectral radiant emittance	W_λ	$W_\lambda \equiv \frac{\partial W}{\partial \lambda}$	$W \cdot cm^{-2} \cdot \mu^{-1}$
Spectral irradiance	H_λ	$H_\lambda \equiv \frac{\partial H}{\partial \lambda}$	$W \cdot cm^{-2} \cdot \mu^{-1}$
Spectral radiance	N_λ	$N_\lambda \equiv \frac{\partial N}{\partial \lambda}$	$W \cdot cm^{-2} \cdot sr^{-1} \cdot \mu^{-1}$
Radiant emissivity	ϵ	Ratio of "emitted" radiant power to that from an ideal blackbody at the same temperature.	
Radiant absorptance	α	Ratio of "absorbed" radiant power to incident radiant power.	
Radiant reflectance	ρ	Ratio of "reflected" radiant power to incident radiant power.	
Radiant transmittance	τ	Ratio of "transmitted" radiant power to incident radiant power.	

Note:

The spectral radiant emissivity $\epsilon(\lambda) \equiv W_\lambda / W_{\lambda, BB} \neq \partial\epsilon/\partial\lambda$. Hence, the subscript notation ϵ_λ, which could be confused with $\partial\epsilon/\partial\lambda$, is not recommended, although it is often used. Similarly, it is recommended that the spectral absorptance, spectral reflectance, and spectral transmittance be written as $\alpha(\lambda)$, $\rho(\lambda)$, and $\tau(\lambda)$, respectively.

Ω = the solid angle filled by the rays along which the radiation is propogated

A = the area of the surface

θ = the angle between the given direction and the normal to the surface

Table 2 (Wolfe, 1965)

EQUIVALENT AIR MASSES FOR SOLAR ALTITUDES 0° TO 90°

	0°	1°	2°	3°	4°	5°	6°	7°	8°	9°
0°	–	26.96	19.79	15.36	12.44	10.40	8.90	7.77	6.88	6.18
10°	5.60	5.12	4.72	4.37	4.08	3.82	3.59	3.39	3.21	3.05
20°	2.90	2.77	2.65	2.55	2.45	2.36	2.27	2.20	2.12	2.06
30°	2.00	1.94	1.88	1.83	1.78	1.74	1.70	1.66	1.62	1.59
40°	1.55	1.52	1.49	1.46	1.44	1.41	1.39	1.37	1.34	1.32
50°	1.30	1.28	1.27	1.25	1.24	1.22	1.20	1.19	1.18	1.17
60°	1.15	1.14	1.13	1.12	1.11	1.10	1.09	1.09	1.08	1.07
70°	1.06	1.06	1.05	1.05	1.04	1.04	1.03	1.03	1.02	1.02
80°	1.02	1.01	1.01	1.01	1.01	1.00	1.00	1.00	1.00	1.00
90°	1.00	–	–	–	–	–	–	–	–	–

*Entries in the table are the air masses for the angles indicated down the left and across the top. For example the air mass for 22° elevation is 2.65.

Table 3 (Hunt et. al., 1950)

Spectral Positions of Infrared Absorption Bands of Minerals and Chemicals

	Wave-Length Range, Microns																
	2-3μ	4μ	5μ	6μ	7μ	8μ	9μ		10μ		11μ		12μ		13μ	14μ	15μ
I. Minerals																	
Carbonates																	
Magnesite, $MgCO_3$	...	4.00 w	5.52 w	6.9 s	...	...	...	...	...	...	11.25 m	11.70 w	...	...	13.33 m	. .	...
Dolomite, $CaMg(CO_3)_2$	...	4.00 w	5.52 w	6.9 s	...	...	...	...	...	...	11.30 m	11.70 w	...	...	13.70 m	...	...
Calcite, $CaCO_3$	...	4.02 w	5.58 w	6.95 s	...	...	...	...	...	...	11.40 m	11.80 w	...	...	...	14.02 m	...
Aragonite, $CaCO_3$	...	4.02 w	5.58 w	6.95 s	...	...	...	...	...	...	11.40 m	11.65 m	...	...	...	14.02 m	...
	...	...	...	...	...	...	...	...	...	...	...	...	...	...	...	14.30 w	...
Rhodochrosite, $MnCO_3$	...	4.05 w	5.58 w	...	7.0 s	...	...	...	...	...	11.50 m	11.95 w	...	...	13.72 m	...	...
Siderite, $FeCO_3$	...	4.05 w	5.58 w	...	7.0 s	...	...	...	...	...	11.50 m	11.95 w	...	...	13.50 m	...	...
Smithsonite, $ZnCO_3$	...	4.05 w	5.58 w	...	7.0 s	...	...	...	...	...	11.47 m	11.90 w	...	...	13.40 m	...	...
Sulfates																	
Gypsum, $CaSO_4.2H_2O$	2.85 m	...	...	6.15 m	7.55 w	8.72 s	9.14 s	9.92 m	...	...	...	...	12.72 w	...	...	...	15.15 m
	...	...	...	...	...	8.97 s	...	...	...	...	...	...	...	...	...	...	...
Gypsum, $CaSO_4$ (dehydrated)	...	...	...	6.90 w	...	8.72 s	9.10 s	9.85 w	...	...	11.42 w	...	...	...	...	14.90 m	...
Barite, $BaSO_4$	...	...	...	6.15 w	7.55 w	8.45 m	9.2 s	...	10.16 m	...	11.30 w	...	12.75 w	...	...	...	15.70 m
	...	...	...	6.80 w	...	8.9 s	...	...	...	...	...	...	...	...	...	...	...
Sulfides																	
Pyrite, FeS_2	...	...	...	...	...	8.9 m	9.7 s	9.9 s	10.95 m	...	...	...	12.6 w	...	...	...	...
Galena, PbS	...	...	...	6.9 m	...	...	9.5 w	...	...	...	11.5 w	...	...	...	...	...	...
Oxides																	
α-Quartz, SiO_2	...	...	5.1 w	6.2 w	...	8.60 s	9.2 s	...	10.95 w	...	...	...	12.52 m	12.82 m	...	14.42 m	...
	...	...	5.38 w	...	...	...	...	...	...	...	...	...	...	...	...	...	...
	...	...	5.6	...	...	...	...	...	...	...	...	...	...	...	...	...	...
	...	...	5.95 w	...	...	...	...	...	...	...	...	...	...	...	...	...	...
Chert, SiO_2	...	...	5.1 w	6.2 w	...	8.60 s	9.2 s	...	...	...	...	...	12.52 m	12.82 m	...	14.42 m	...
	...	...	5.38 w	...	...	...	...	...	...	...	...	...	...	...	...	...	...
	...	...	5.6 w	...	...	...	...	...	...	...	...	...	...	...	...	...	...
	...	...	5.95 w	...	...	...	...	...	...	...	...	...	...	...	...	...	...
Opal, $SiO_2.nH_2O$	3.0 w	...	5.38 w	6.1 w	...	8.2 m	9.2 m	...	10.5 m	...	...	...	12.55 m	...	...	...	...
Hematite, Fe_2O_3	...	...	...	...	7.05 w	...	...	...	10.2 s	...	...	...	12.3 w	...	13.3 m	...	...
Ilmenite, $(Fe,Mg)OTiO_2$	...	...	...	...	...	...	...	...	10.0 m	10.3 m	...	...	...	...	...	...	16 s
Silicates																	
Olivine, $(Mg,Fe)_2SiO_4$	2.75 w	...	...	6.1 w	...	...	...	...	10.0 s	10.5 s	11.2 s	11.90 m	...	...	13.1 w	...	...
Garnet, $Fe_3Al_2Si_3O_{12}$ (almandite)	...	...	...	6.9 w	...	...	9.8 m	...	10.35 s	...	11.13 s	11.47 s	...	...	...	...	...
Augite, $CaMg(SiO_3)_2$	...	...	...	6.9 w	...	...	9.37 s	9.8 s	10.38 s	10.9 m	11.45 s	...	...	...	...	14.95 m	15.8 m
Tremolite, $(OH)_2Ca_2Mg_5(Si_4O_{11})_2$	...	...	...	...	...	...	9.0 s	9.9 s	10.55 s	10.85 m	...	...	...	...	13.15 m	14.6 m	...
	...	...	...	...	...	...	9.3 s	...	...	...	...	...	...	...	...	14.95 m	...
Actinolite, $(OH)_2Ca_2(Mg,Fe)_5(Si_4O_{11})_2$	...	...	...	...	...	...	9.0 s	10.1 s	10.5 s	10.85 s	...	...	...	...	13.15 m	14.6 m	...
	...	...	...	...	...	...	9.35 s	...	...	...	...	...	...	...	...	14.95 m	...
Hornblende	...	...	...	6.15 w	7.55 w	...	...	9.8 s	...	...	...	...	12.75 w	...	...	14.95 m	15.05 w
Wollastonite, $CaSiO_3$	...	...	...	...	...	...	9.10 s	9.75 s	10.33 s	10.72 s	11.05 s	...	...	...	...	14.7 m	15.5 m
	...	...	...	...	...	...	9.40 s	...	...	...	...	...	...	...	...	...	...
Biotite, $K(Mg,Fe)_3(AlSi_3O_{10})(OH)_2$	...	...	...	...	...	...	...	...	10.0 s	10.3 s	...	...	12.8 w	...	...	14.3 m	...
Muscovite, $KAl_2(AlSi_3O_{10})(OH)_2$	2.78 m	...	...	...	...	...	9.35 s	9.7 s	...	...	11.0 m	...	12.1 w	12.5 w	13.35 m	14.8 w	...
Talc, $Mg_3(Si_4O_{10})(OH)_2$	...	...	...	...	...	...	...	9.8 s	...	...	...	...	...	...	...	14.9 m	15.1 w
Microcline, $KAlSi_3O_8$	...	...	...	6.15 w	7.55 w	8.80 s	9.1 s	9.9 s	...	...	...	...	12.95 m	...	13.70 m	...	15.42 w
	...	...	...	...	...	...	9.5 s	...	...	...	...	...	...	...	...	...	...
Albite, $NaAlSi_3O_8$	...	...	...	6.8 w	...	8.70 s	9.1 s	9.9 s	...	...	...	...	12.68 m	...	13.10 m	...	15.4 m
	...	...	...	...	...	...	9.7 s	...	...	...	...	...	...	...	13.40 m	...	...
	...	...	...	...	...	...	...	...	...	...	...	...	...	...	13.80 m	...	...
Oligoclase, (80% albite, 20% anorthite)	...	...	...	6.15 m	7.55 w	8.7 s	9.1 s	9.9 s	...	...	...	...	12.70 m	...	13.15 m	...	15.6 m
	...	...	...	...	...	...	9.6 s	...	...	...	...	...	...	...	13.8 m	...	...
Anorthite, $CaAl_2Si_2O_8$	...	...	...	6.9 w	...	...	9.1 m	...	10.0 s	10.9 w	...	...	12.2 w	...	13.2 m	14.6 w	...
	...	...	...	...	...	...	...	...	10.5 s	...	...	...	...	...	13.7 w	...	...
Nepheline, $NaAlSiO_4$	...	...	...	6.1 w	...	...	9.2 s	...	10.1 s	...	...	...	...	...	13.0 m	14.05 m	15.0 m
	...	...	...	6.6 w	...	...	...	...	...	...	...	...	...	...	13.60 m	14.5 m	...
Clay minerals																	
Kaolinite, $Al_2Si_2O_5(OH)_4$	2.73 m	...	...	6.0 w	7.55 w	8.93 s	9.65 s	9.90 s	10.68 m	10.95 s	...	...	12.50 m	12.65 m	13.3 w	14.5 m	...
	...	...	...	6.1 w	...	...	...	...	...	...	...	...	...	...	...	...	...
Illite	2.78 to 3.2 m	...	...	6.0 w 6.1 w	7.55 w	8.95 m	9.7 s	...	...	10.95 m	...	...	12.05 w	...	13.3 w	...	...
Montmorillonite	2.8 to 3.2 m	...	...	6.15 m	7.55 w	8.95 m	9.6 s	...	...	10.95 m	11.4 m	11.85 m	...	12.75 w	...	...	...

Table 4 (Middleton, 1952)

K FROM THE MIE THEORY, FOR VARIOUS VALUES OF α AND n

	n			
α	1.33	1.44	1.55	2.00
0.5	0.00676	0.0115	0.0172	0.0457
0.6	.0138	.0238	.0359	.343
1.0	.0938	.1670	.258	.796
1.2	.171	.306	.476	1.611
1.5	.322	.577	.924	4.231
1.8	.523	.994	1.698	3.722
2.0	0.710	1.365	2.205	4.770
2.4	1.126	1.896	2.736	4.097
2.5	1.212	2.029	3.024	3.776
3.0	1.754	2.911	3.689	3.000
3.6	2.376	3.627	4.367	2.022
4.0	2.826	3.850	4.138	1.738
4.8	3.490	4.010	3.563	2.565
5.0	3.592	3.984	3.688	2.856
6.0	3.888	3.611	2.222	2.683

ADDITIONAL VALUES FOR $n = 1.33$

α	K	α	K	α	K	α	K
7.0	3.722	11.5	1.858	15.5	2.740	19.75	1.976
8.0	3.282	11.75	1.758	16.0	2.870	20.0	2.092
9.0	2.738	12.0	1.670	16.25	2.872	20.25	2.180
9.5	2.394	12.125	1.776	16.5	2.850	20.5	2.078
10.0	2.152	12.250	1.892	16.75	2.810	21.0	1.834
10.25	2.052	12.333	1.936	17.0	2.632	22.0	1.922
10.5	1.886	12.5	1.938	17.125	2.704	24.0	2.438
10.625	1.918	12.6	1.822	17.375	2.820		
10.75	1.930	12.75	1.850	17.5	2.738		
10.875	1.832	13.0	2.012	18.0	2.598		
11.0	1.740	13.5	2.192	18.5	2.432		
11.125	1.728	14.0	2.474	19.0	2.218		
11.333	1.734	14.5	2.528	19.25	2.090		
11.4	1.768	15.0	2.744	19.5	1.998		

Table 5 (Valley, 1965)

Density ($\mu g\ m^{-3}$) of solid and liquid particles.

Environment		Wind Speed (mile h^{-1})	Content ($\mu g\ m^{-3}$)
			Sea Spray
Maritime Air		10	4
		20	10
		35	30
		60	100
			Aerosol
Continental Air	Country		50
	Medium-sized Town		100 to 200
	Large City		500 to 1000

Table 6 (Valley, 1965)

Increase in aerosol concentrations due to various extreme conditions.

Condition	Factor by which Increased	Applicable Size Range
Smog in Large Cities	Up to 30	Whole size range
Dust Clouds over Deserts (Excluding surface layer)	Up to 100	Sizes larger than 0.1 μ
Surf Areas along Coast	Up to 100	All sea spray particles
Storm Areas over Sea	Up to 10	Particles less than 10 μ
	Up to 100	Particles larger than 10 μ

Table 7 (Brennan et. al., 1970)

Integrated Directional Reflectance and Relative Anisotropy as Measured with an Aircraft-borne MRIR over Various Earth Surfaces

Flt. No.	Type of Surface	Surface Alt. (10^3 FT.)	Aircraft Alt. (MSL)	Range of Solar Zenith Angle ζ_o (degrees)	Directional Reflectance $\bar{R}(\zeta_o)$ %(.2-4μ)	%(.55-.85μ)	Anisotropy Factor χ (.2-4μ)	(.55-.85μ)
1966: 12	Desoto National Forest	0.2	37	51.6 - 68.6	18.0	18.6	1.15	1.18
14	Strato Cumulus Over Forest	6.3	41	54.9 - 72.4	51.5	61.9	1.08	1.09
34	Strato Cumulus Over Pacific Ocean	2.3	40	41.0 - 58.1	27.7	35.2	1.49	1.62
35	Pacific Ocean		35	44.6 - 50.5	7.2	9.2	1.83	1.45
36	Strato Cumulus Over Pacific Ocean		40	50.7 - 58.7	33.0	39.0	1.34	1.27
37	Strato Cumulus Over Pacific Ocean		25	68.4 - 75.7	32.0	45.6	2.04	2.08
1967: 1	Strato Cumulus Over Pacific Ocean	4.5	25	61.2 - 69.2	48.2	57.3	1.02	1.21
1	Strato Cumulus Over Pacific Ocean	4.5	35.3	71.4 - 79.0	41.1	51.2	1.31	1.09
3	Strato Cumulus Over Pacific Ocean	10.0	25	22.0 - 24.0	34.5	41.5	1.57	1.47
11	Farmland and Wooded Areas with Patches of Stratus	0.5	33	11.6 - 13.3	13.7	11.4	0.87	0.91
11	Gulf of Mexico		28	29.5 - 35.5	6.1	8.0	0.97	0.85

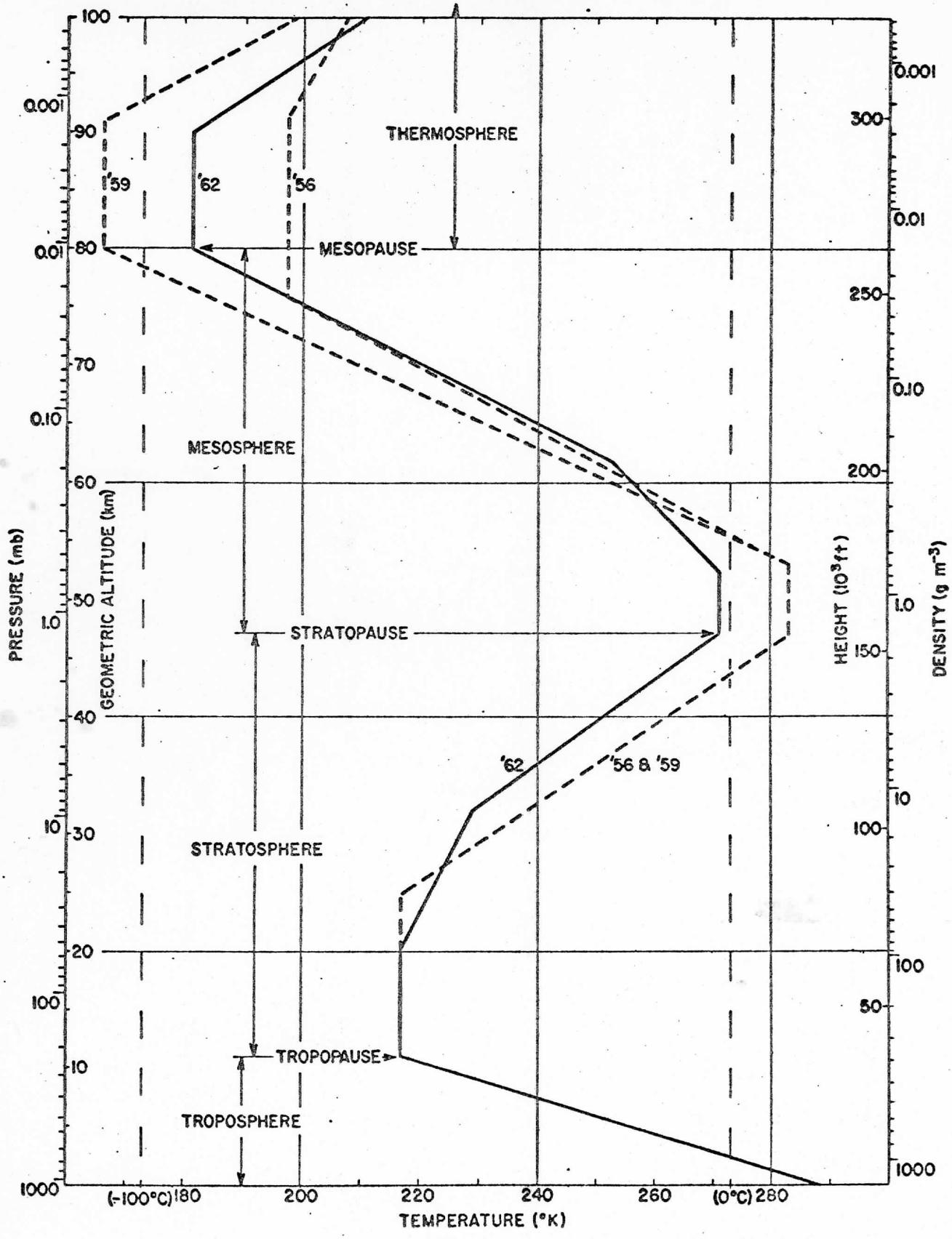
THERMOSPHERE
MESOPAUSE
MESOSPHERE
STRATOPAUSE
STRATOSPHERE
TROPOPAUSE
TROPOSPHERE
'59
'62
'56
'62
'56 & '59
PRESSURE (mb)
GEOMETRIC ALTITUDE (km)
HEIGHT (10^3 ft)
DENSITY (g m^{-3})
TEMPERATURE (°K)
(-100°C)
(0°C)

Figure 1

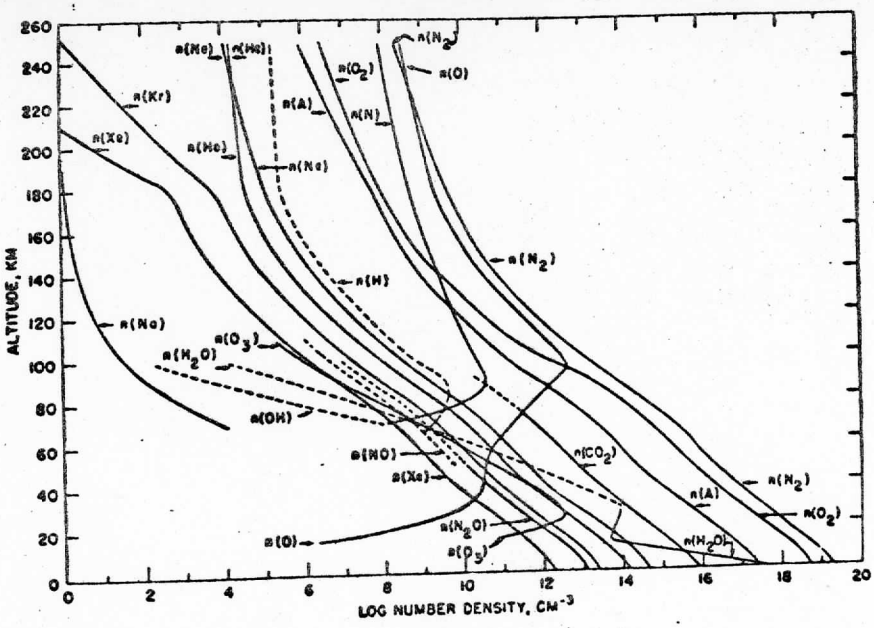
ALTITUDE, KM
LOG NUMBER DENSITY, CM⁻³
n(Ne)
n(He)
n(Kr)
n(Xe)
n(Ar)
n(N)
n(O₂)
n(O)
n(N₂)
n(H)
n(Na)
n(O₃)
n(H₂O)
n(OH)
n(NO)
n(CO₂)
n(N₂O)

Figure 2

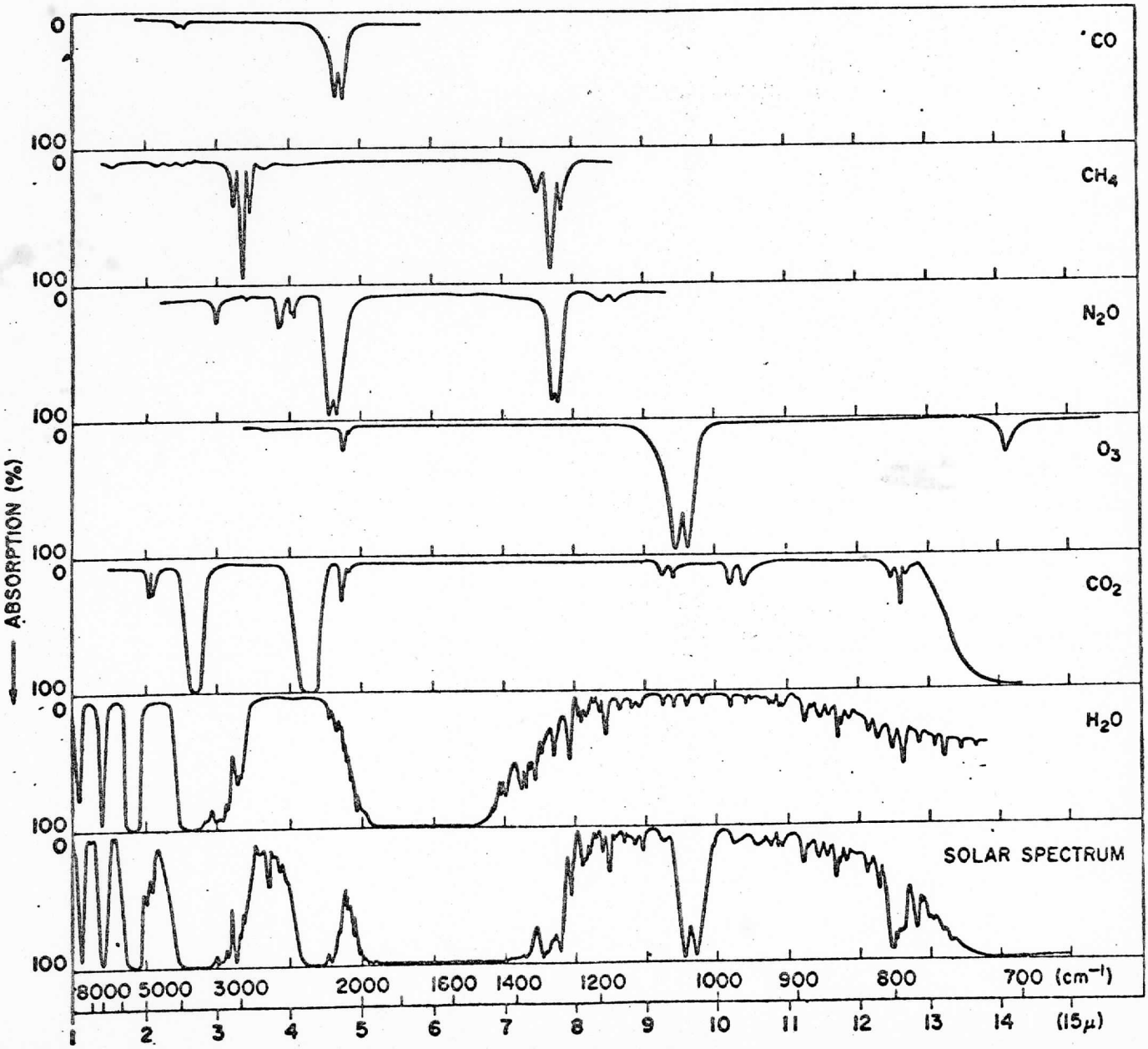
CO
CH₄
N₂O
O₃
CO₂
H₂O
SOLAR SPECTRUM
ABSORPTION (%)
8000 5000 3000 2000 1600 1400 1200 1000 900 800 700 (cm⁻¹)
1 2 3 4 5 6 7 8 9 10 11 12 13 14 (15μ)

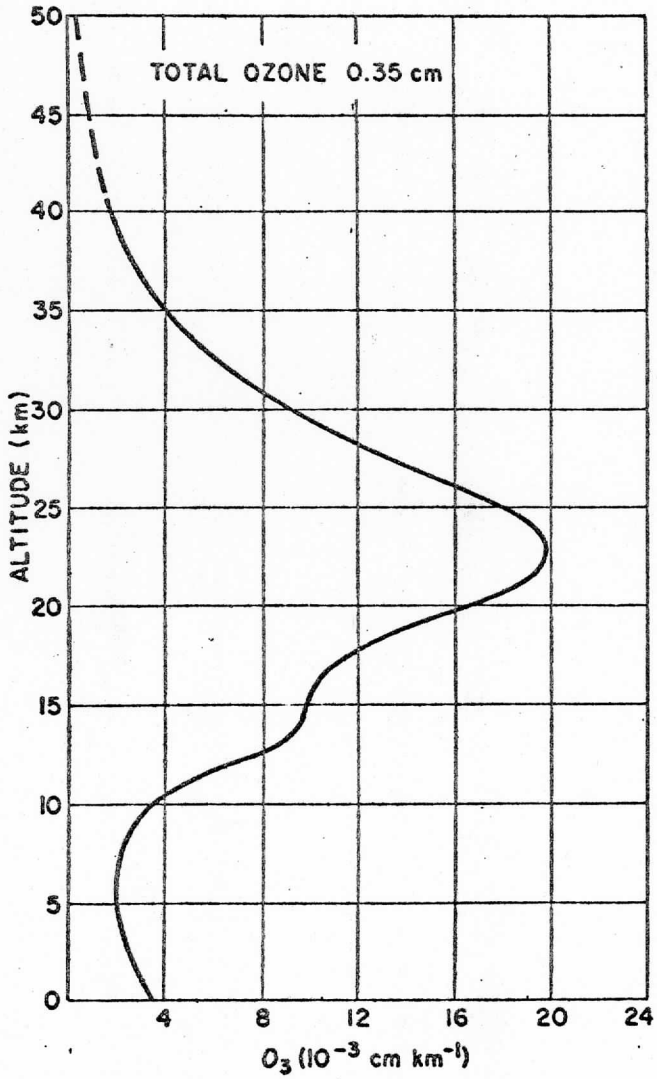
TOTAL OZONE 0.35 cm
ALTITUDE (km)
50
45
40
35
30
25
20
15
10
5
0
4
8
12
16
20
24
O_3 (10^{-3} cm km^{-1})

Figure 4

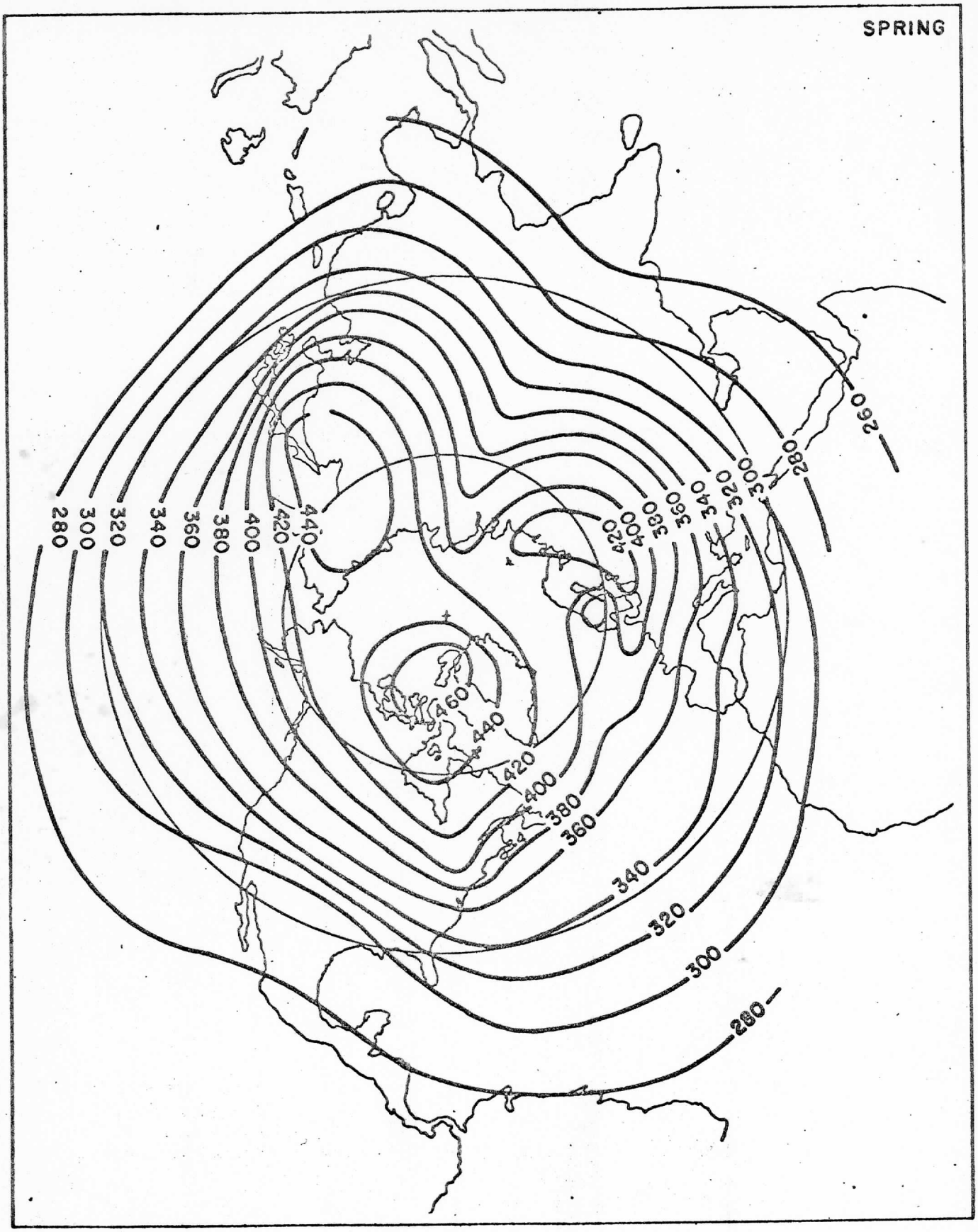
SPRING
280
300
320
340
360
380
400
420
440
460
260
280
300
320
340
360
380
400
420
440
460
420
400
380
360
340
320
300
280

Figure 5

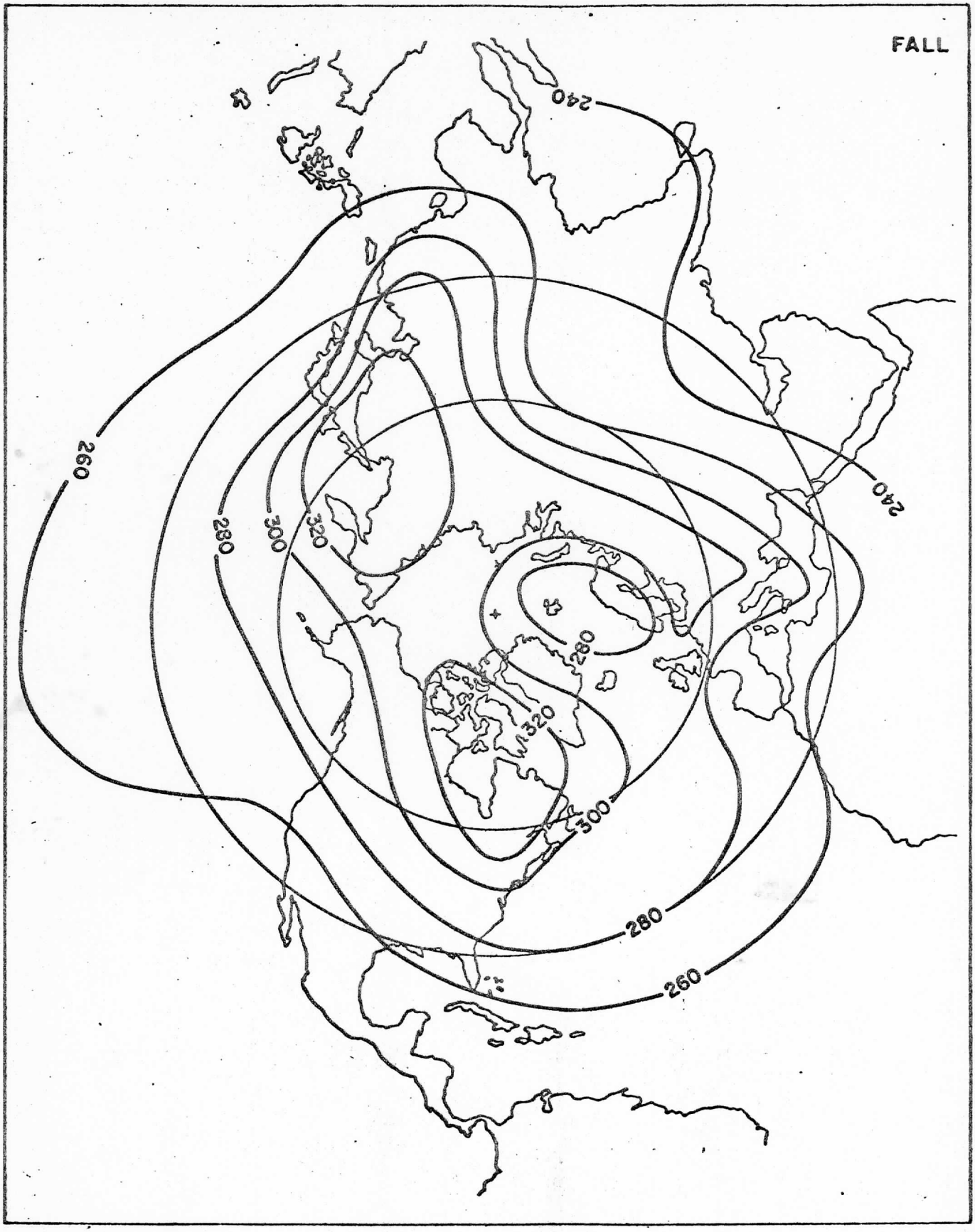

Figure 6

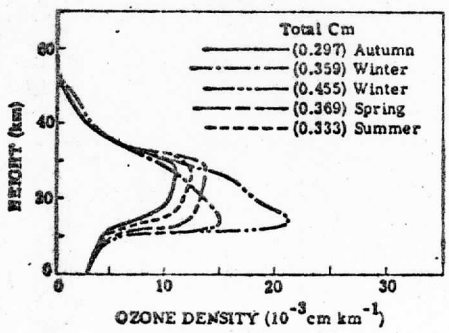

Figure 7

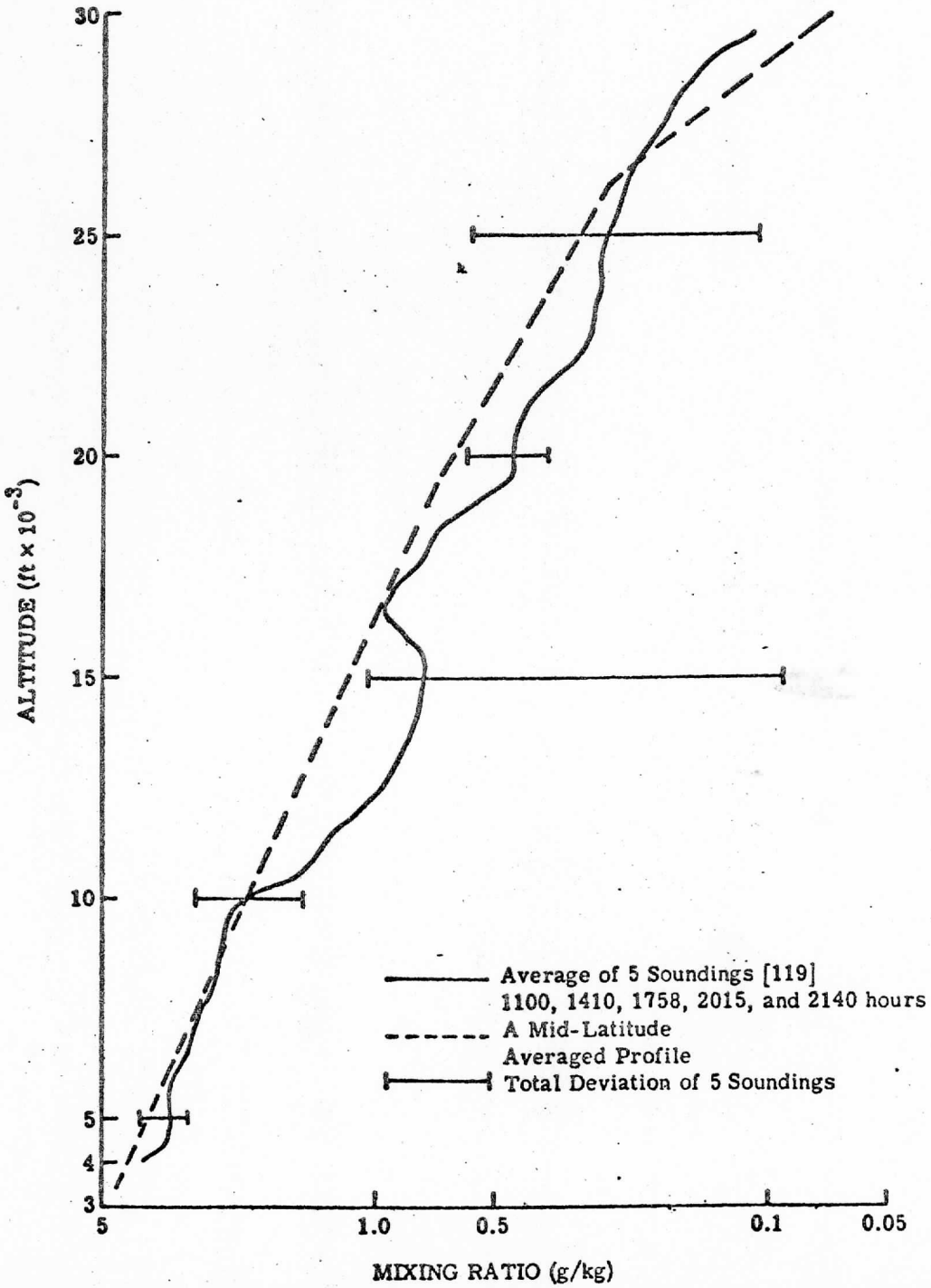

Figure 8

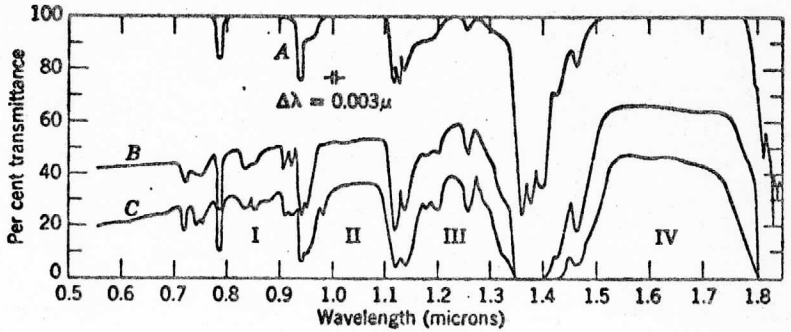

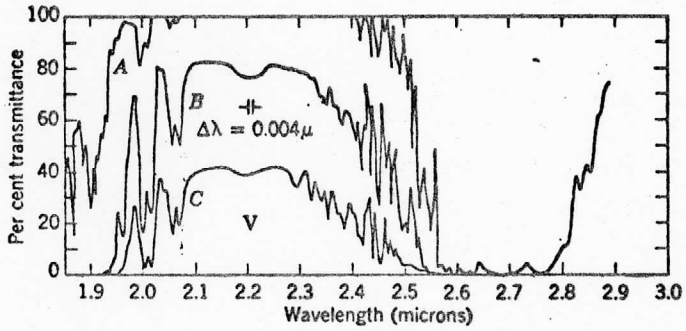

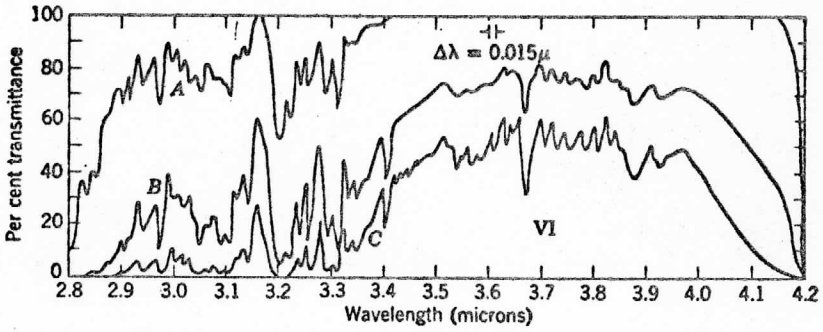

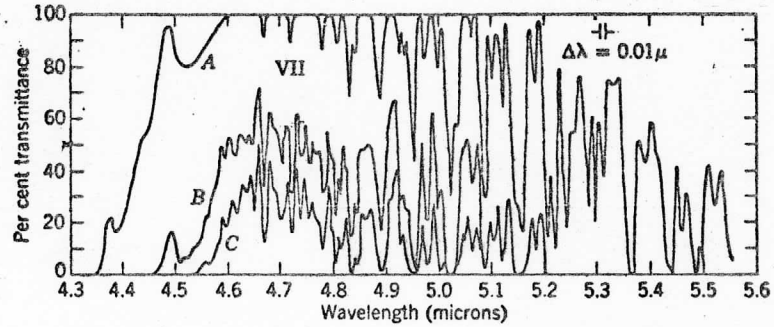

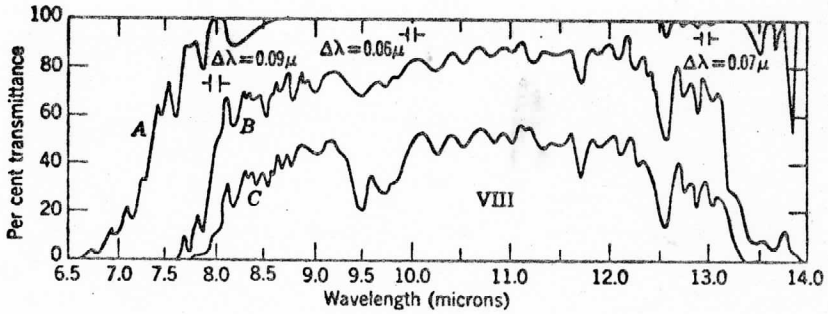

Curve	Path Length	Date	Time	Temp.	R.H.	Precipitable Water	Visual Range
A	1000 ft	3-20-56	3 P.M.	37° F	62%	1.1 mm	22 miles
B	3.4 miles	3-20-56	10 P.M.	34.5° F	47%	13.7 mm	16 miles
C	10.1 miles	3-21-56	12 A.M.	40.5° F	48%	52.0 mm	24 miles

Window Definitions

I	0.72 to 0.94 μ	V	1.90 to 2.70 μ
II	0.94 to 1.13 μ	VI	2.70 to 4.30 μ
III	1.13 to 1.38 μ	VII	4.30 to 6.0 μ
IV	1.38 to 1.90 μ	VIII	6.0 to 15.0 μ

Figure 9

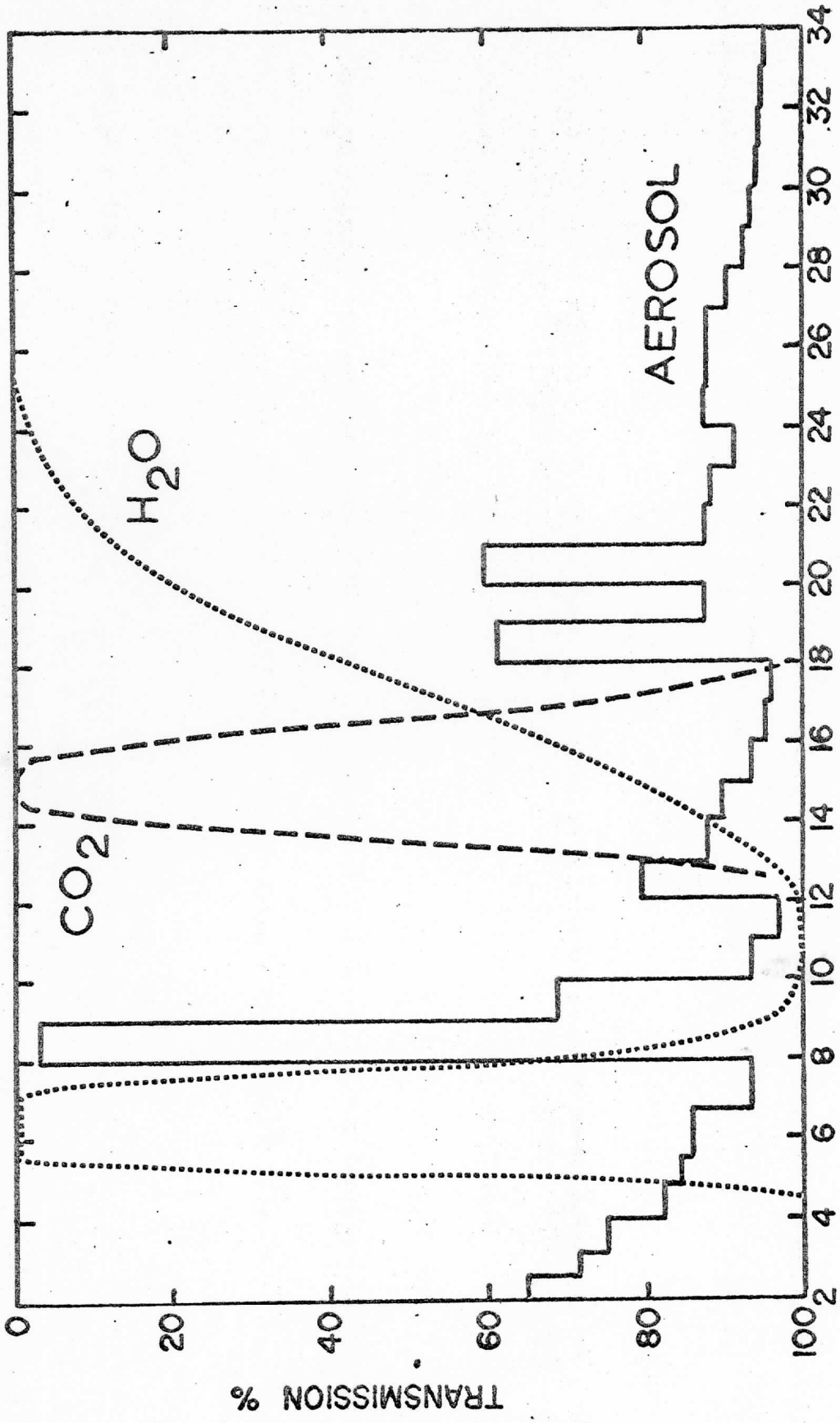
TRANSMISSION %
0
20
40
60
80
100
2
4
6
8
10
12
14
16
18
20
22
24
26
28
30
32
34
WAVELENGTH, MICRONS
H_2O
CO_2
AEROSOL

Figure 10

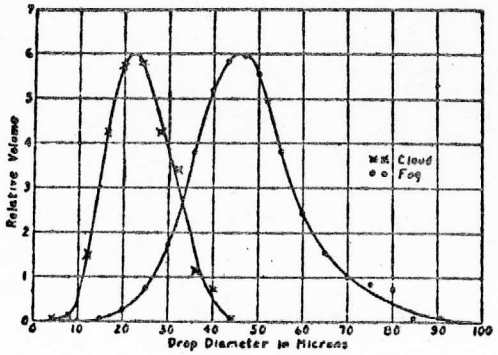

Figure 11

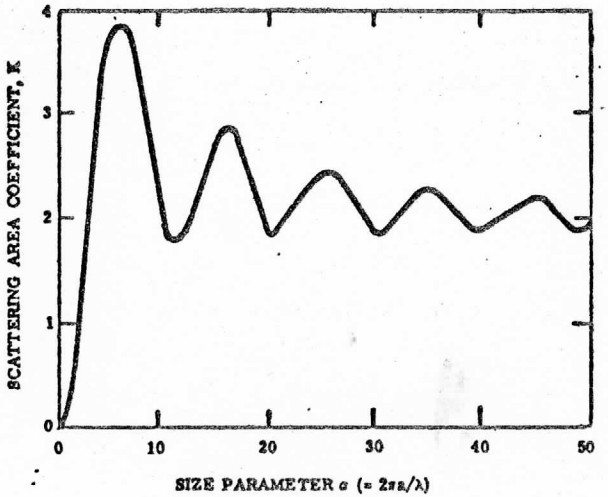

Figure 12

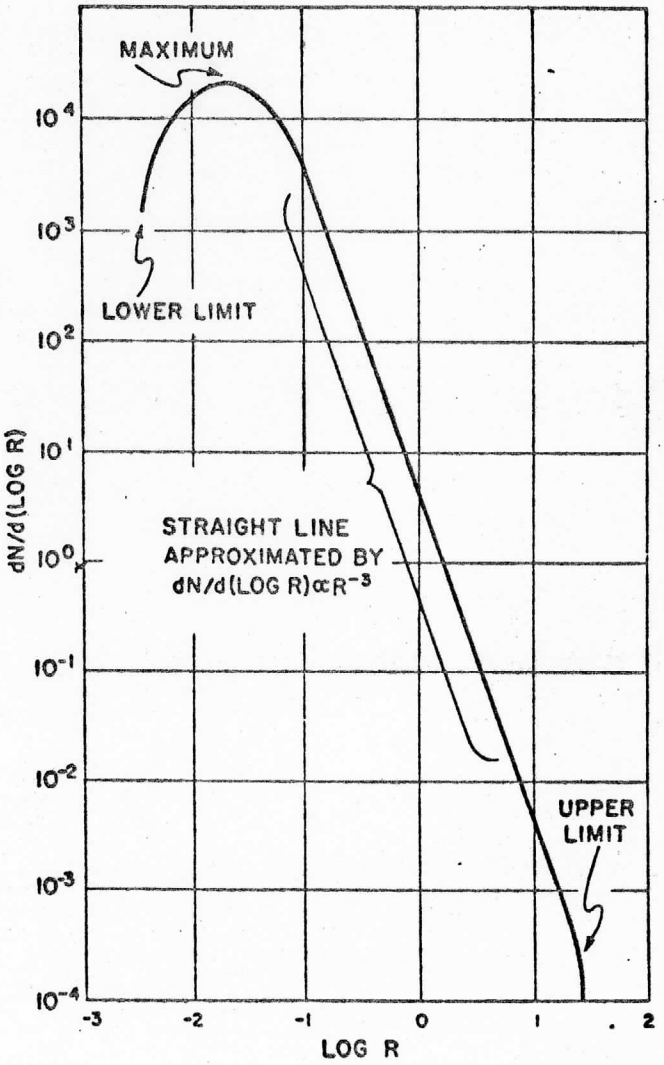

Figure 13

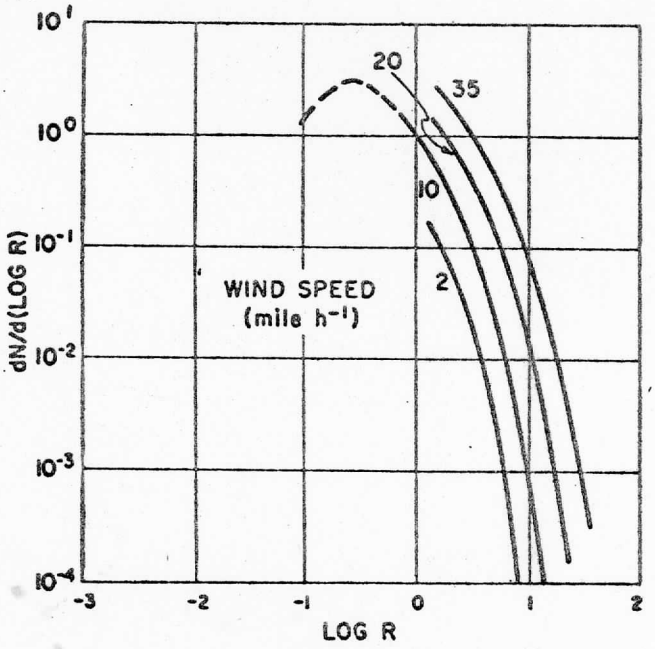

Figure 14

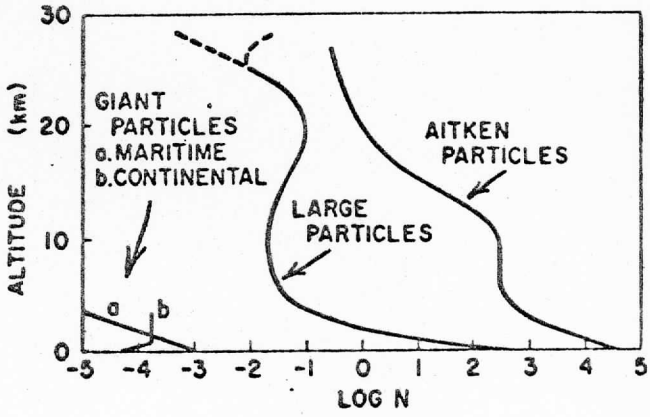

Figure 15

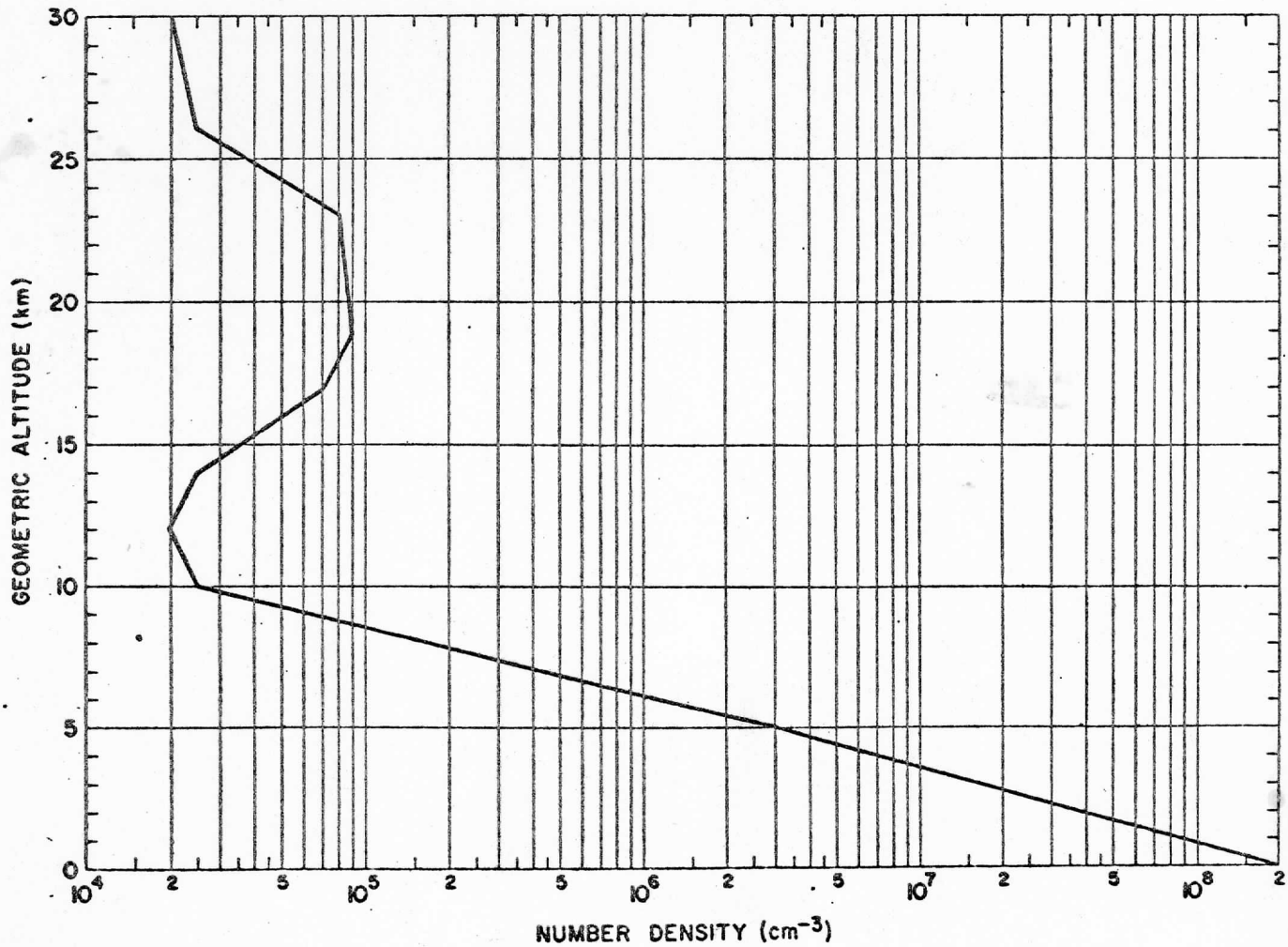

Figure 16

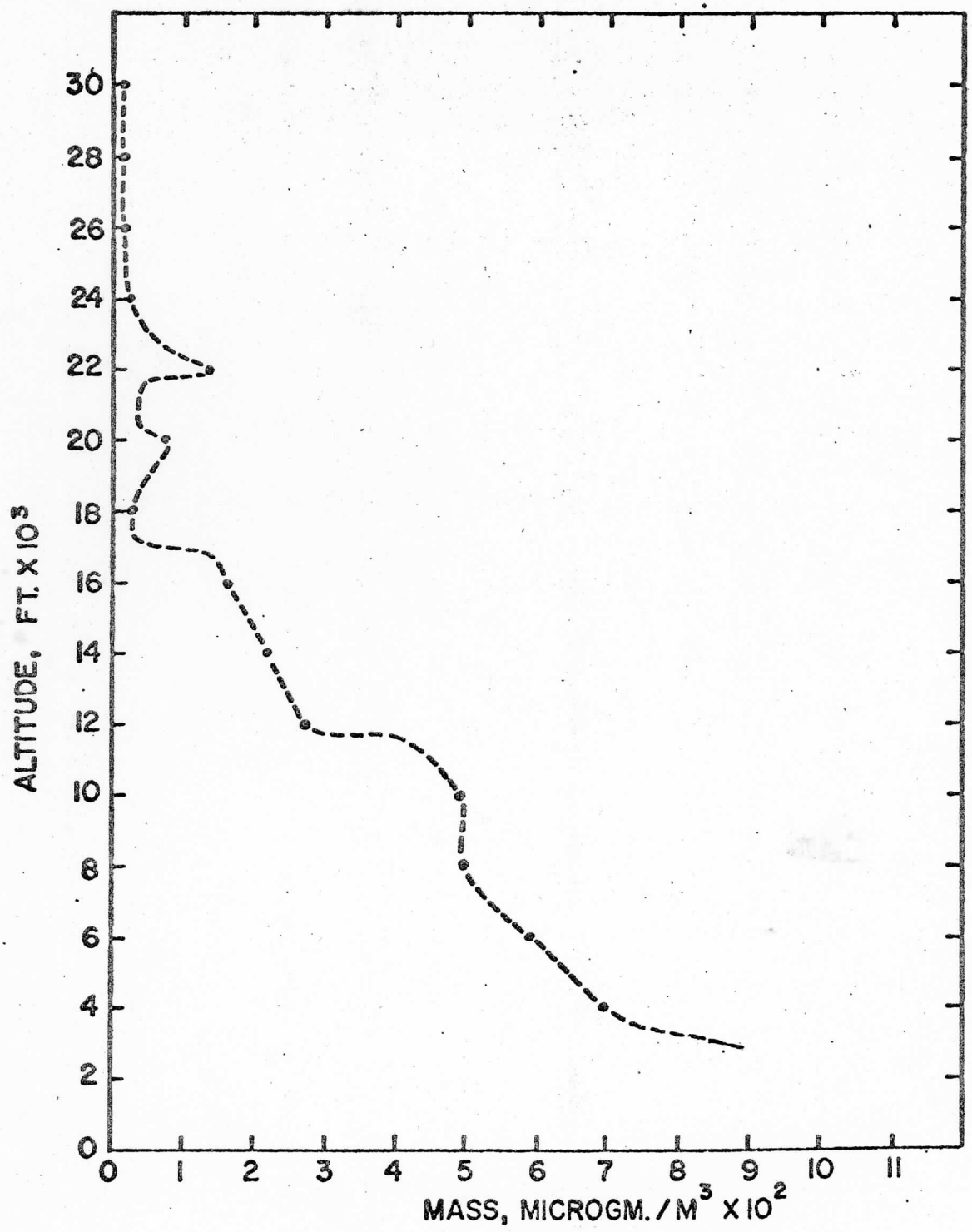
ALTITUDE, FT. X 10³
30
28
26
24
22
20
18
16
14
12
10
8
6
4
2
0
0
1
2
3
4
5
6
7
8
9
10
11
MASS, MICROGM./M³ X 10²

Figure 17

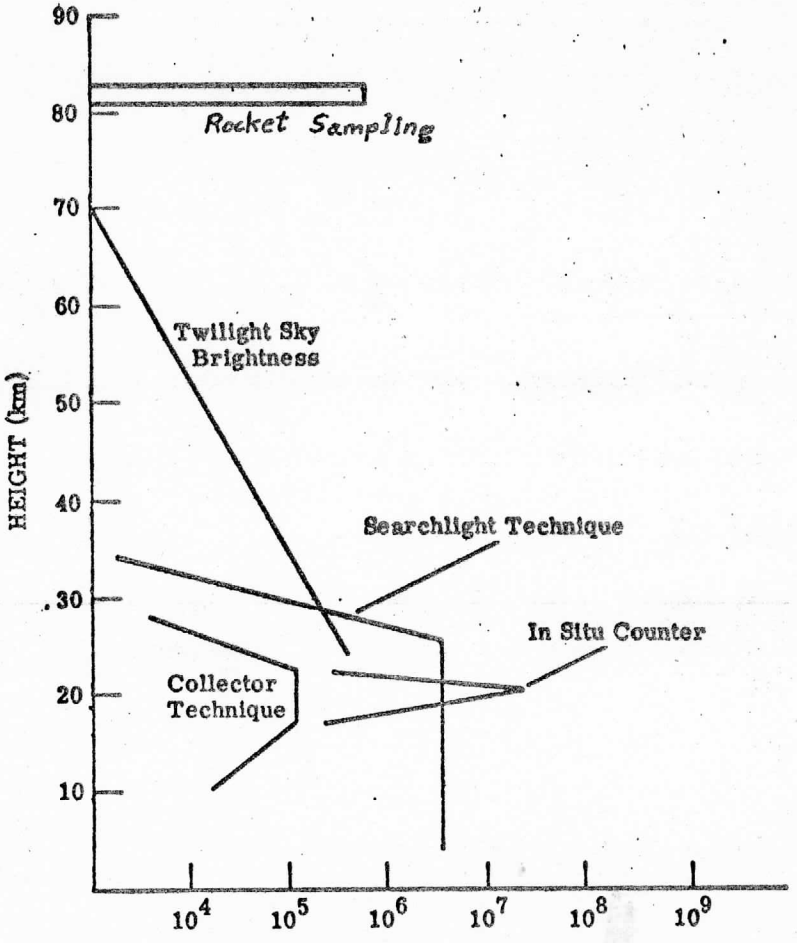

Figure 18

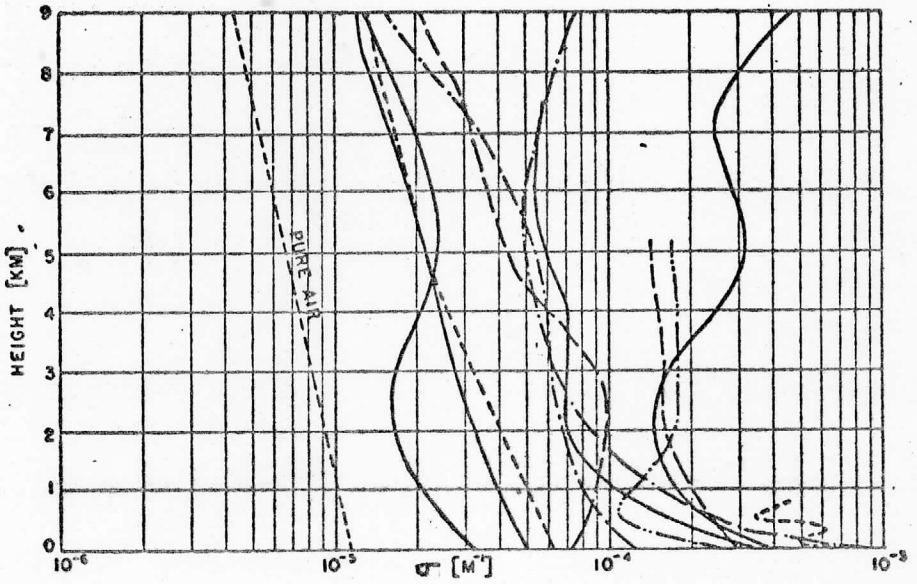

Figure 19

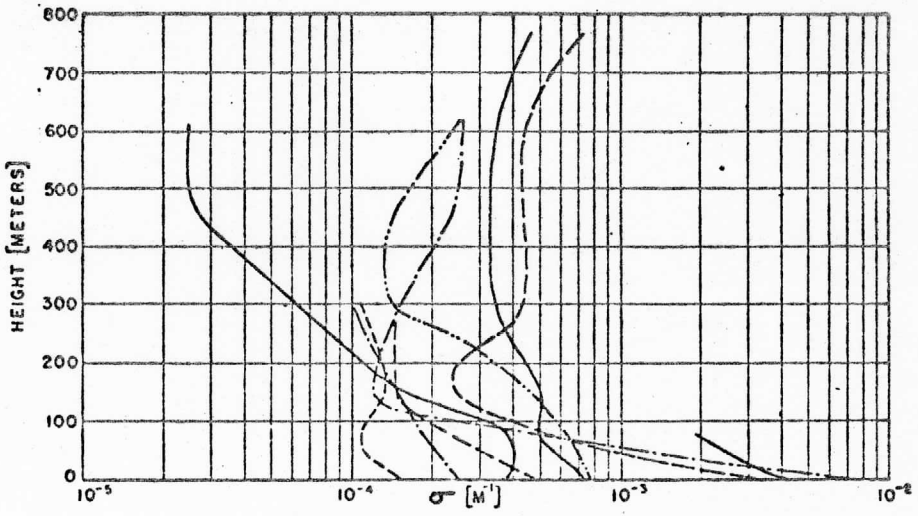

Figure 20

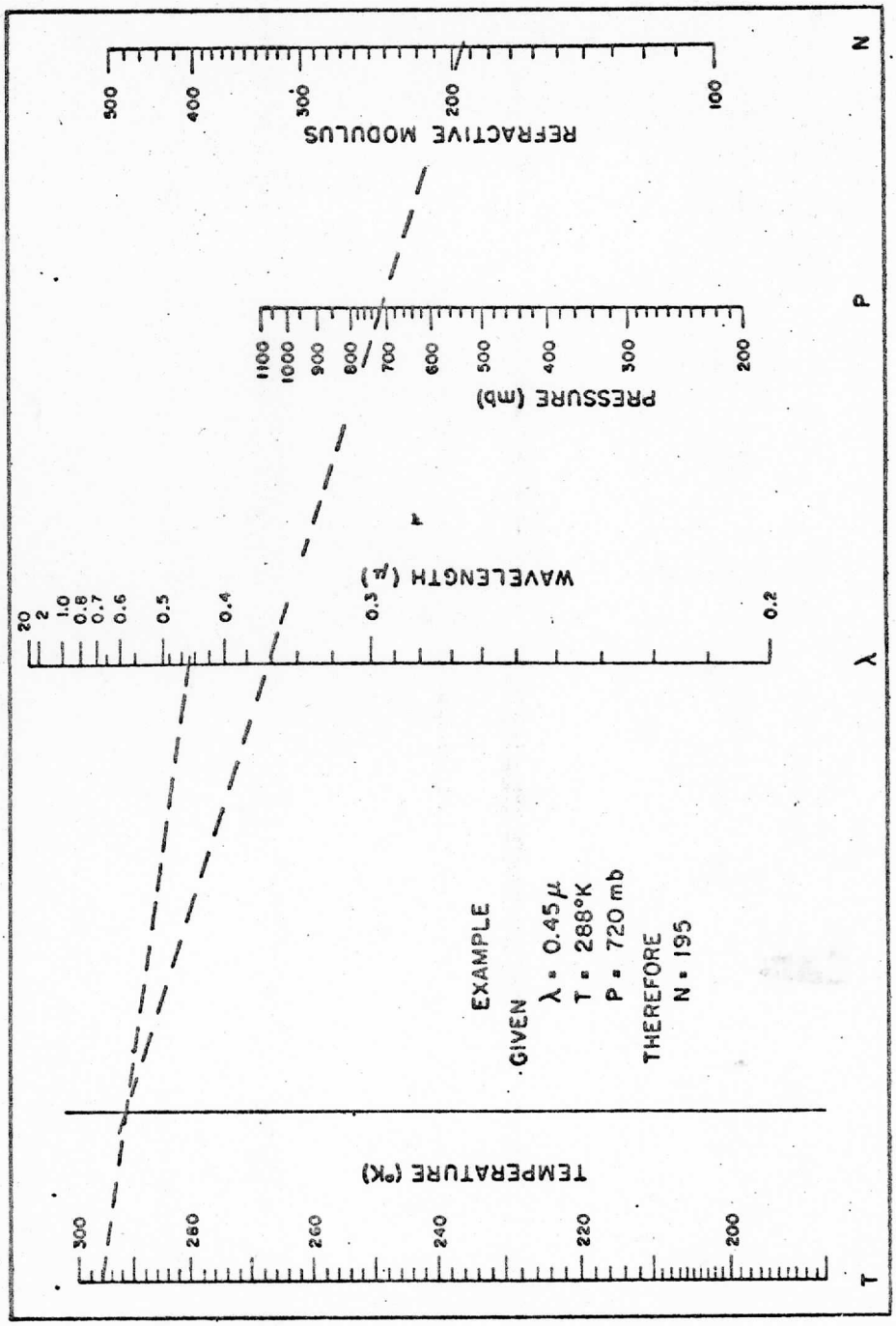
N
REFRACTIVE MODULUS
500
400
300
200
100
P
PRESSURE (mb)
1100
1000
900
800
700
600
500
400
300
200
λ
WAVELENGTH (μ)
20
2
1.0
0.8
0.7
0.6
0.5
0.4
0.3
0.2
EXAMPLE
GIVEN
λ = 0.45μ
T = 288°K
P = 720 mb
THEREFORE
N = 195
T
TEMPERATURE (°K)
300
280
260
240
220
200

Figure 21

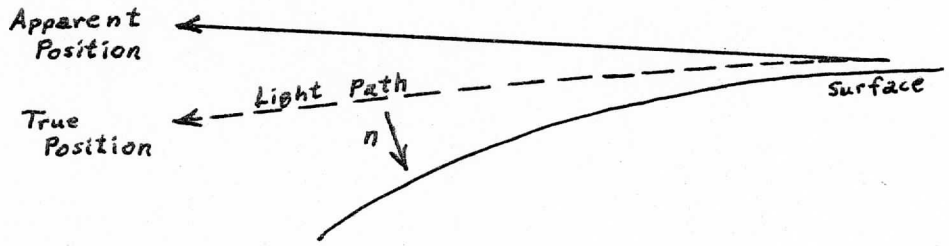

Figure 22

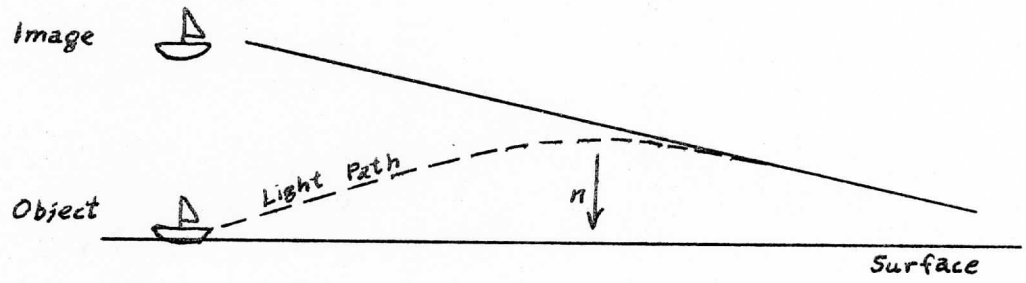

Figure 23

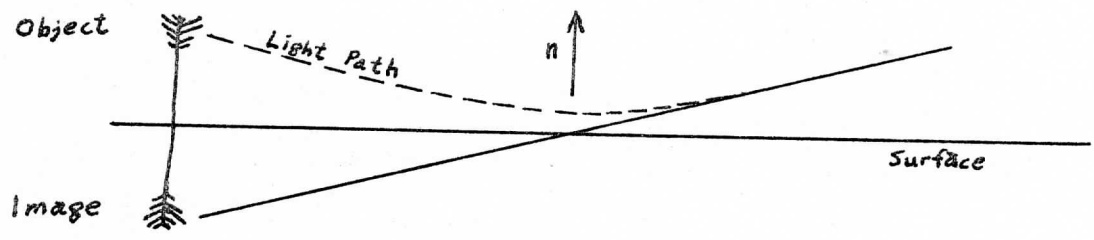

Figure 24

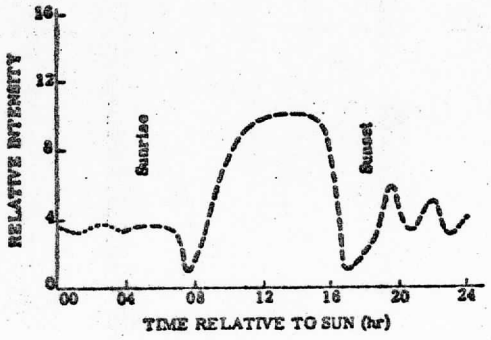

Figure 25

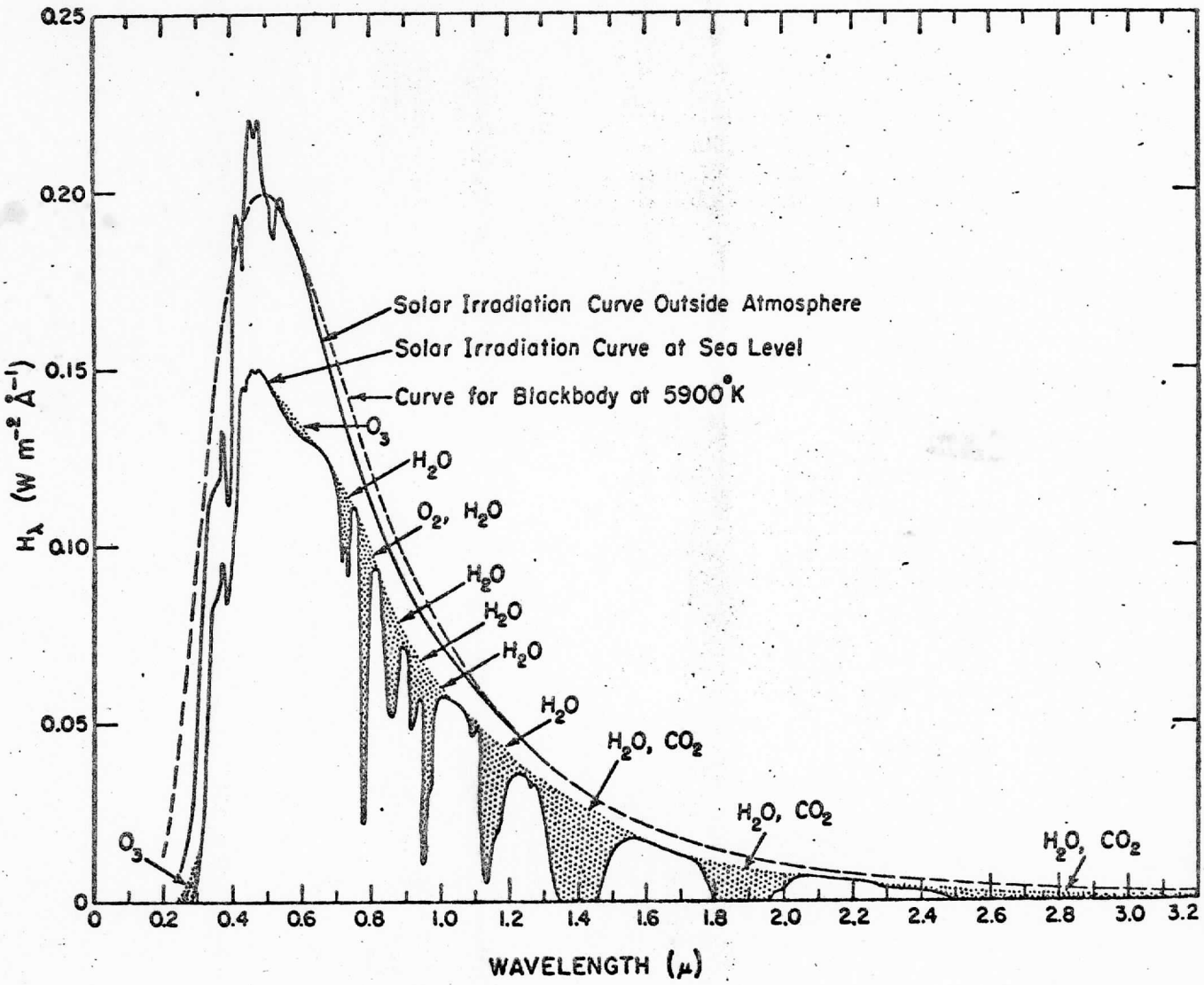

Figure 26

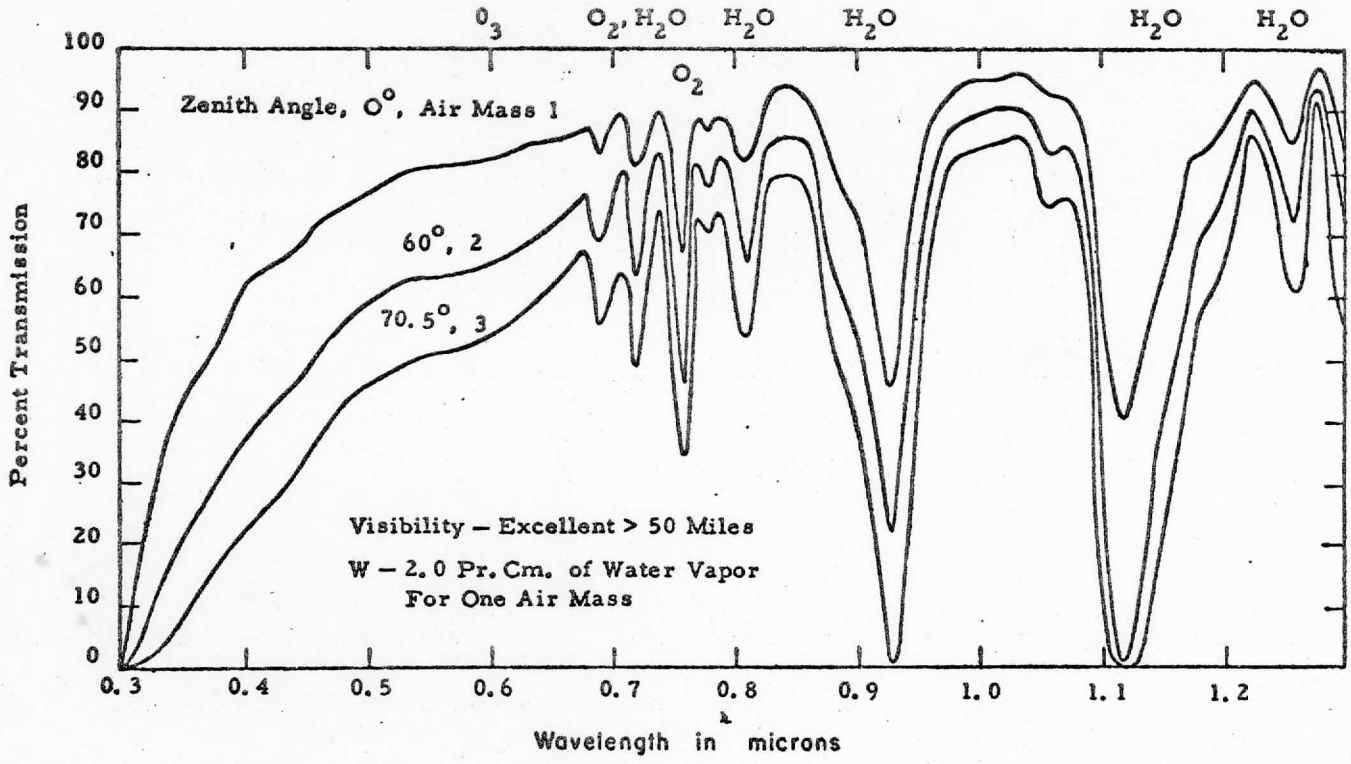

Figure 27

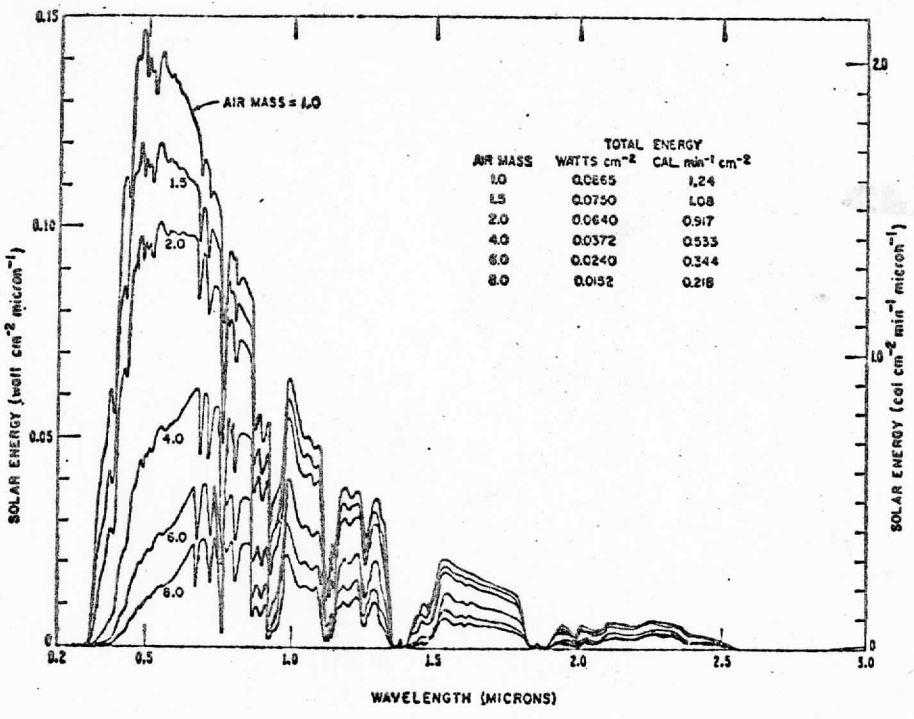

Figure 28

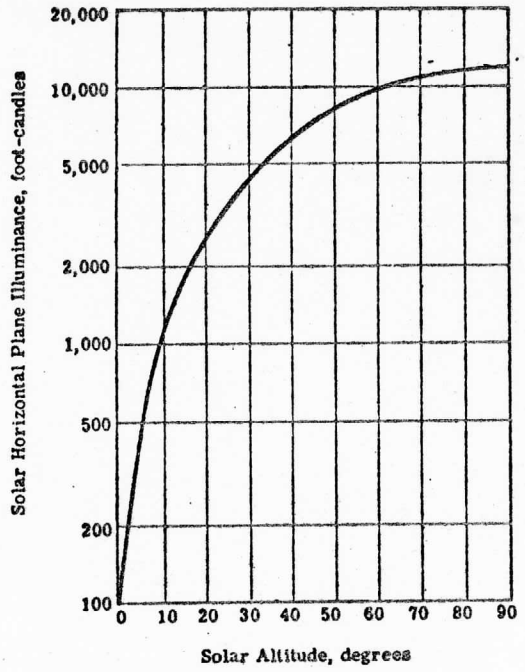

Figure 29

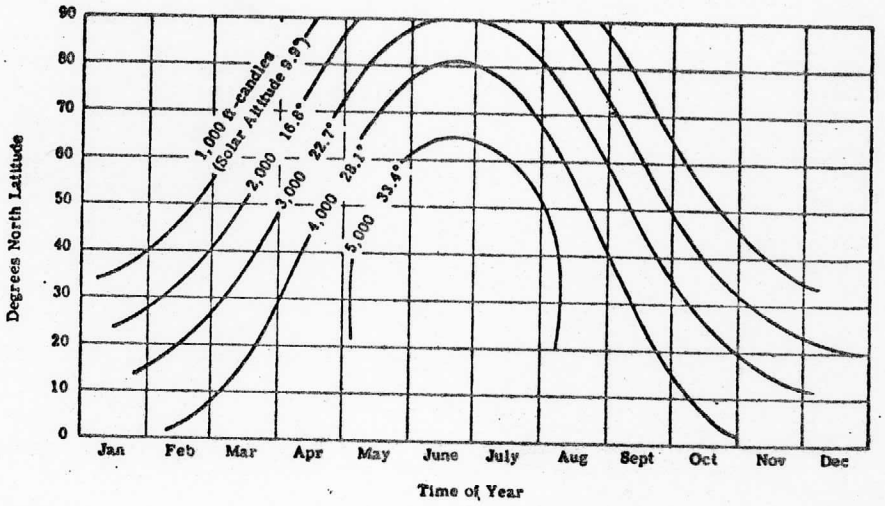

Figure 31

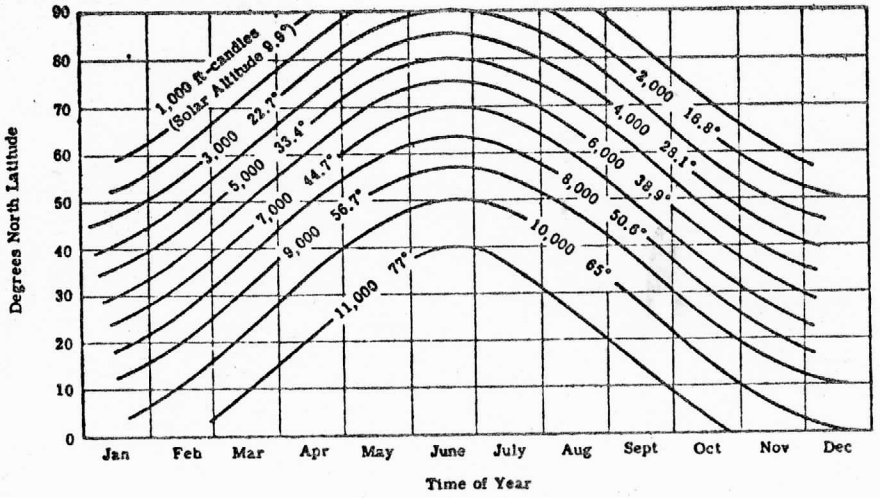

Figure 30

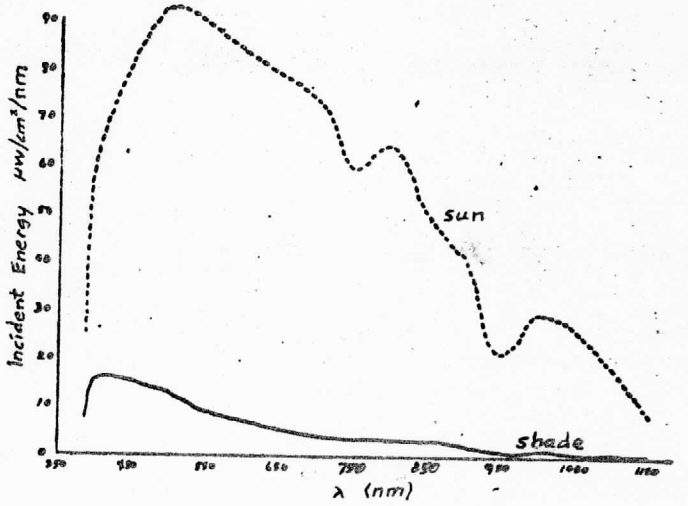

Figure 32

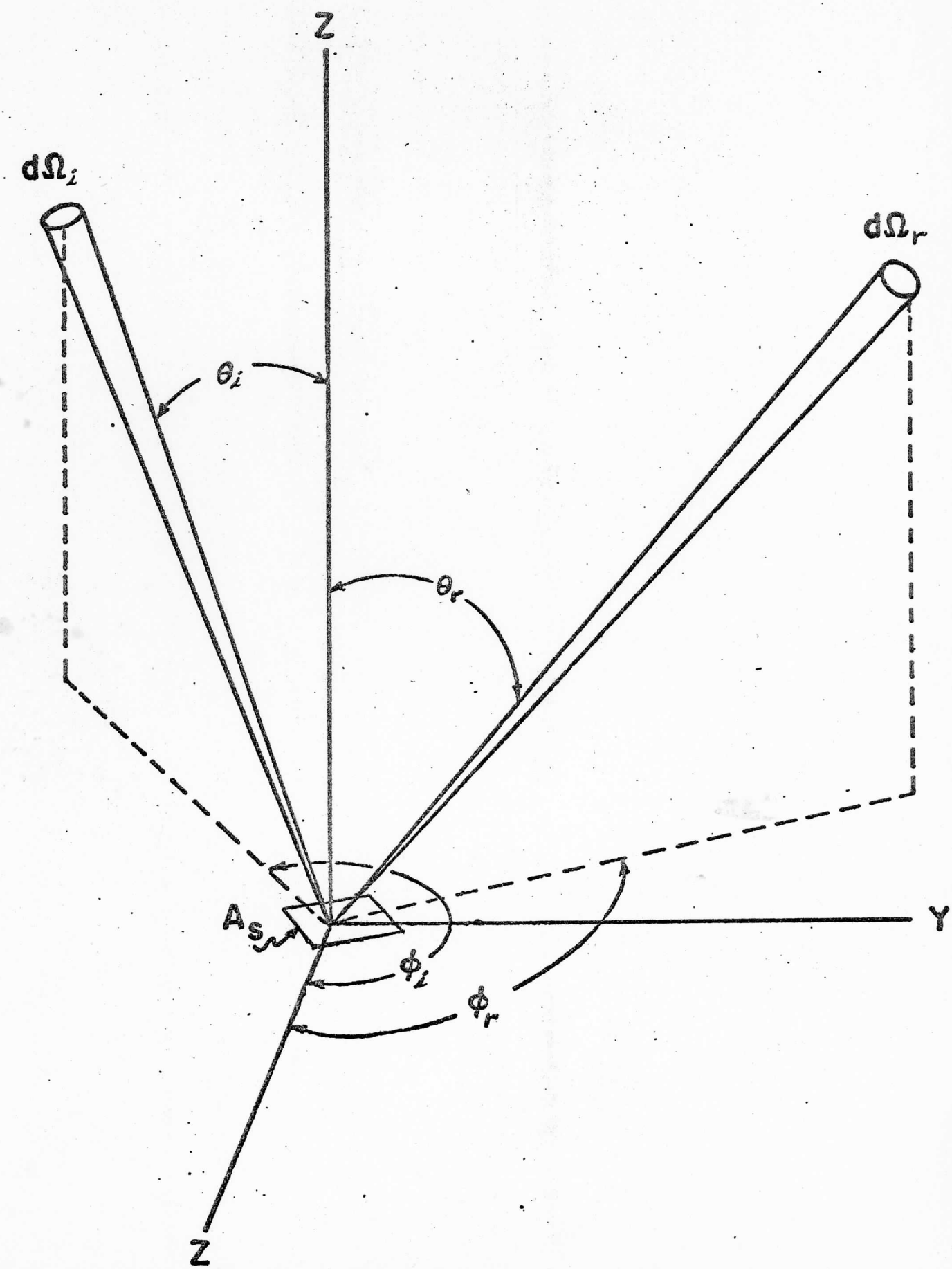

Figure 33

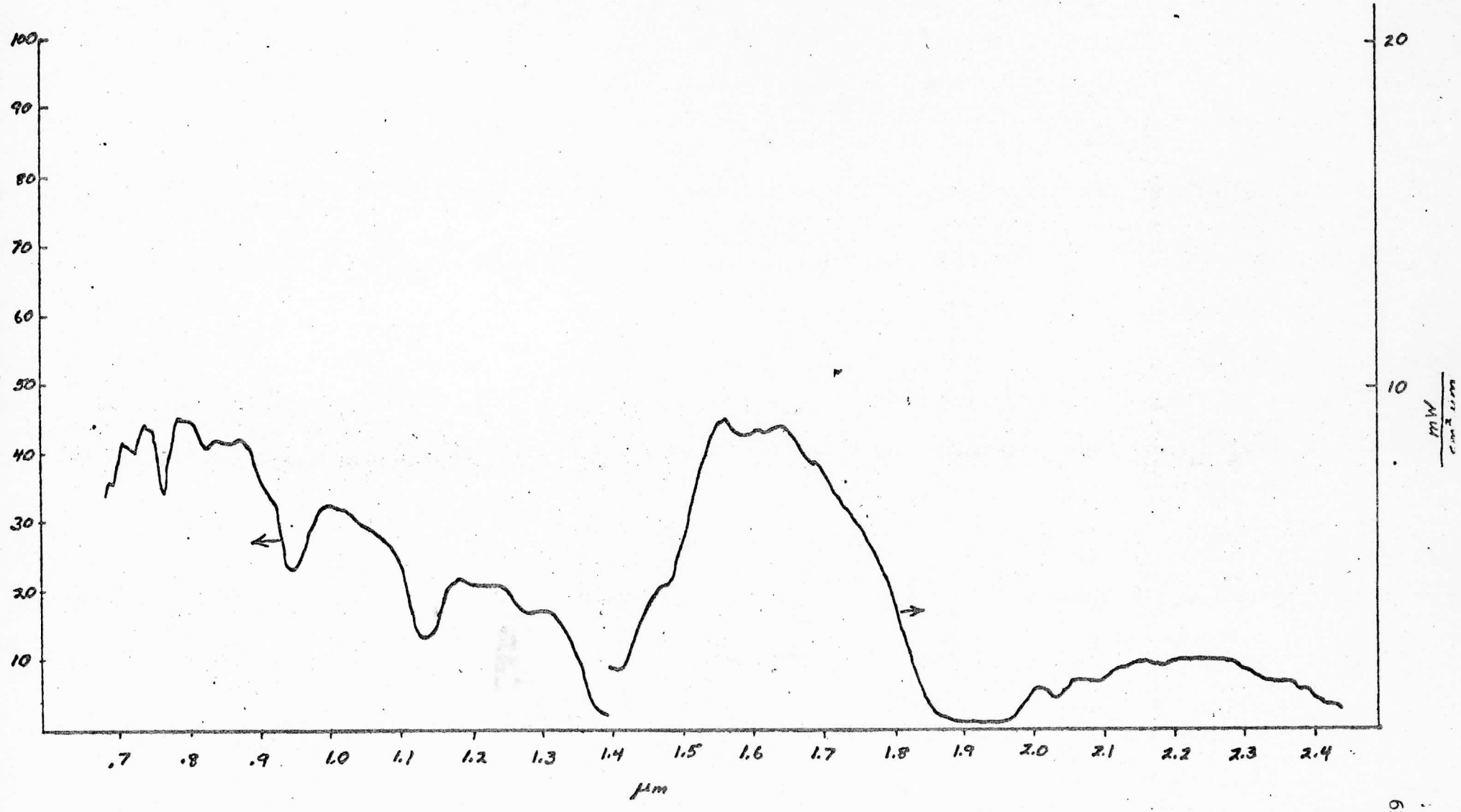
100
90
80
70
60
50
40
30
20
10
20
10
.7
.8
.9
1.0
1.1
1.2
1.3
1.4
1.5
1.6
1.7
1.8
1.9
2.0
2.1
2.2
2.3
2.4
μm

Figure 34

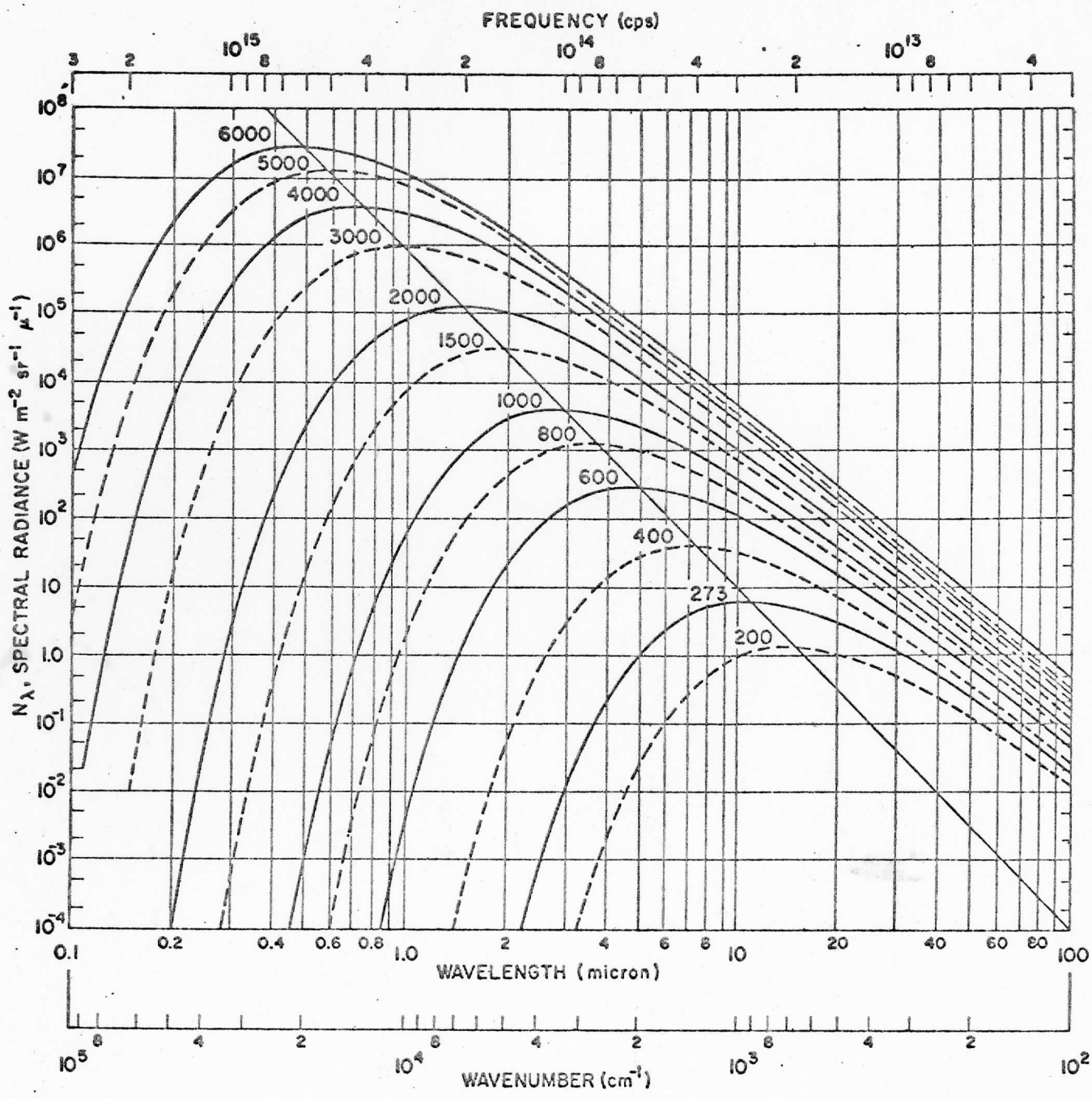
FREQUENCY (cps)
N_λ, SPECTRAL RADIANCE (W m^{-2} sr^{-1} μ^{-1})
6000
5000
4000
3000
2000
1500
1000
800
600
400
273
200
WAVELENGTH (micron)
WAVENUMBER (cm^{-1})

Figure 35

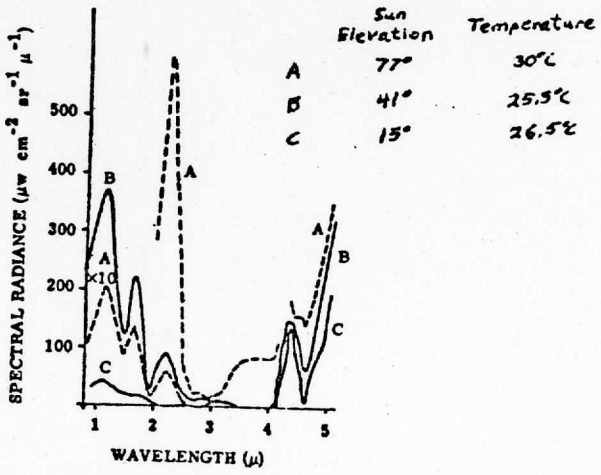

Figure 36

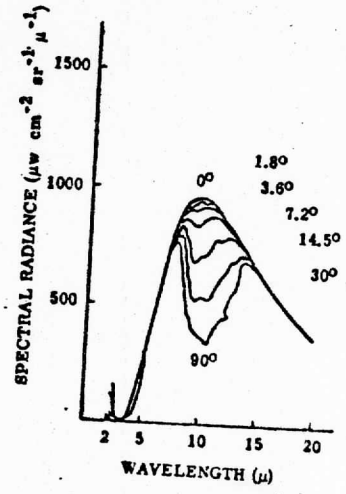

Figure 37

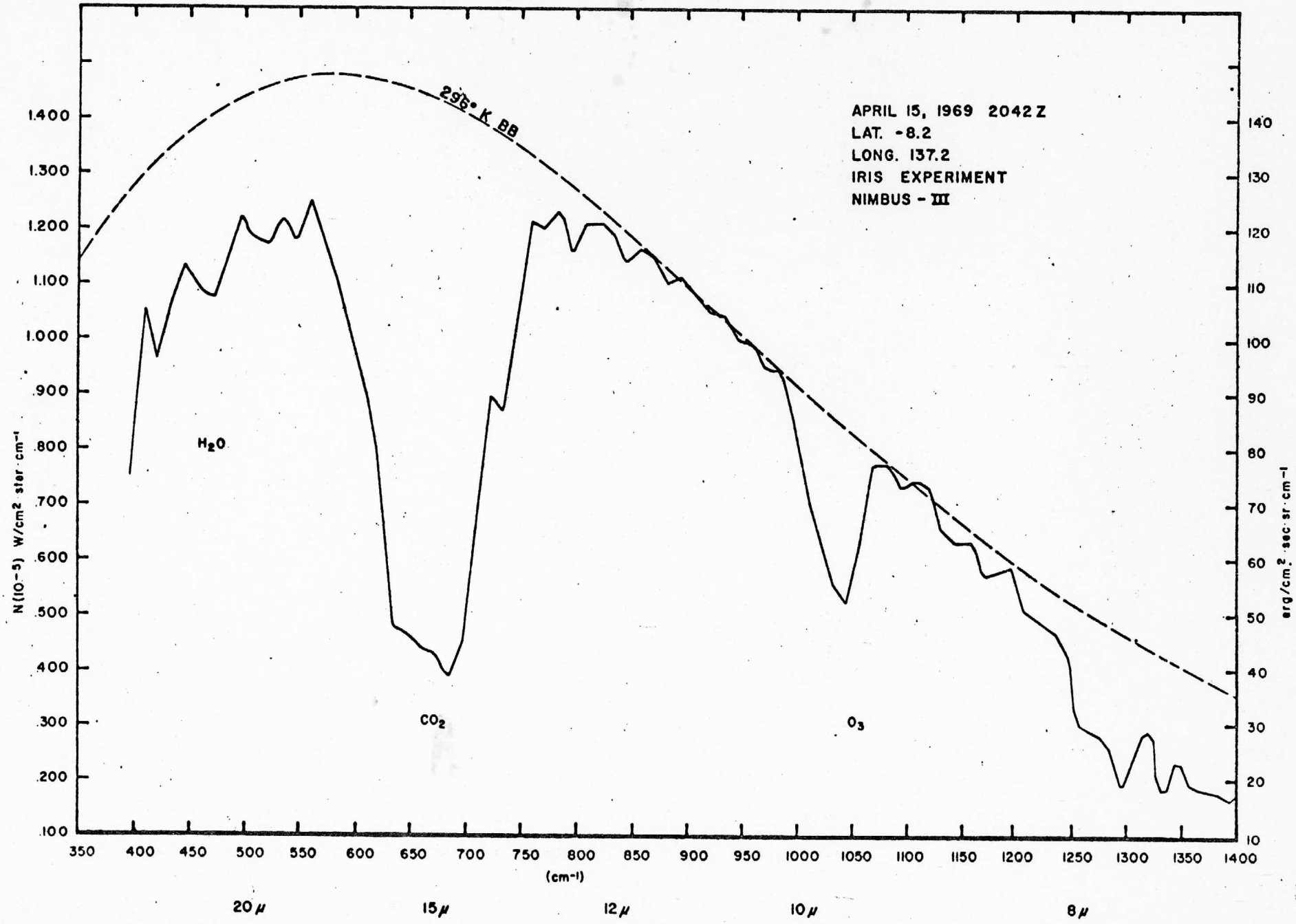
296° K BB
APRIL 15, 1969 2042 Z
LAT. -8.2
LONG. 137.2
IRIS EXPERIMENT
NIMBUS - III
H2O
CO2
O3
N(10-5) W/cm2 ster cm-1
erg/cm2 sec sr cm-1
(cm-1)
20 μ
15 μ
12 μ
10 μ
8 μ

Figure 38

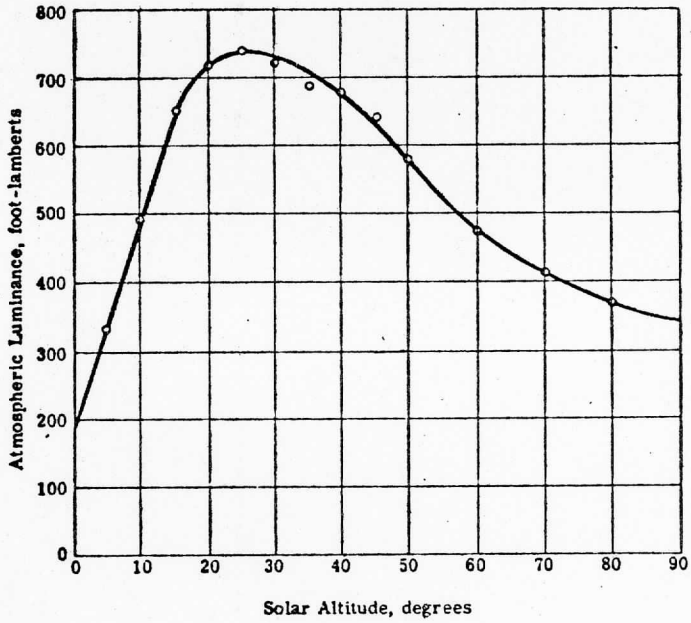

Figure 39

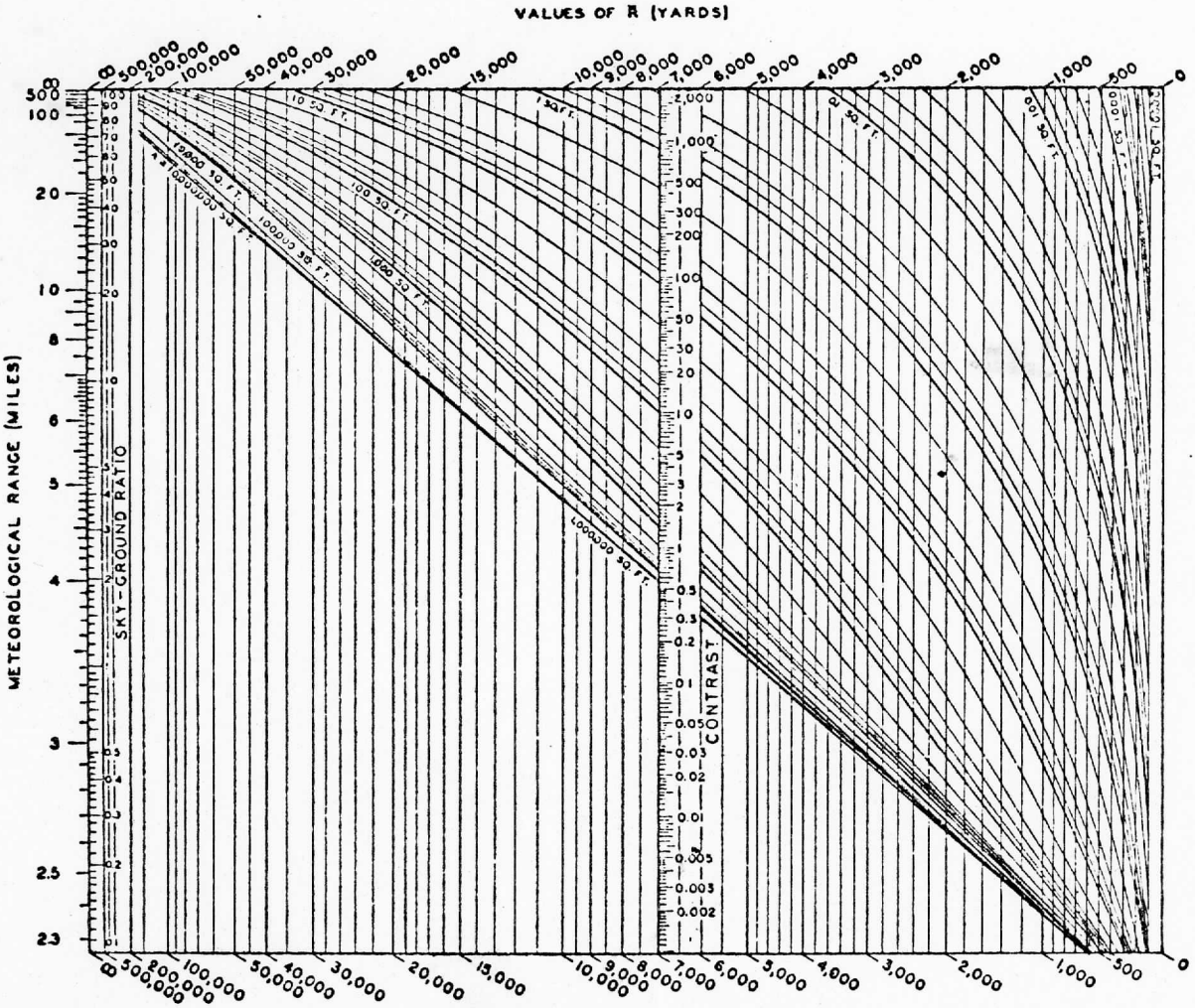

Figure 40

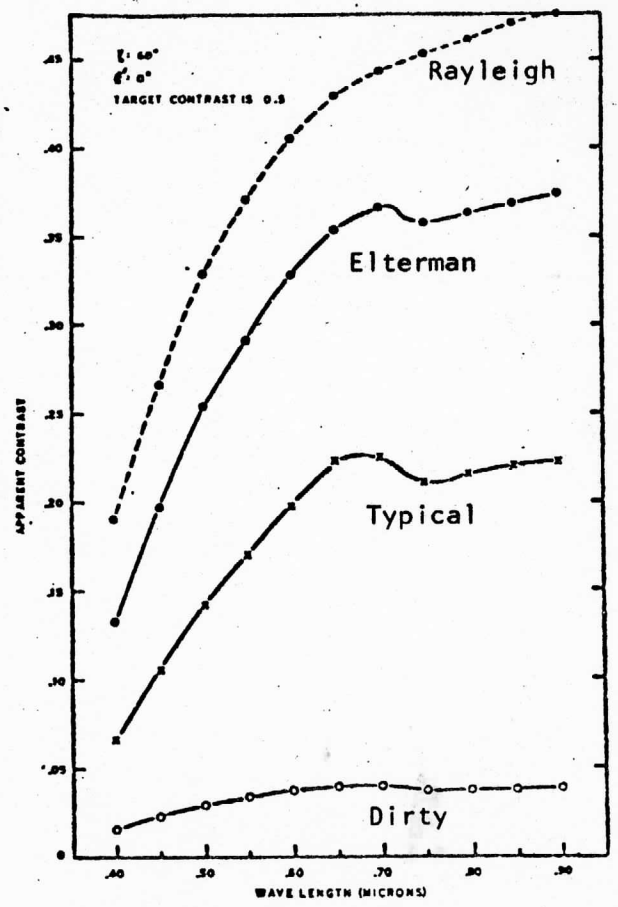

Figure 41

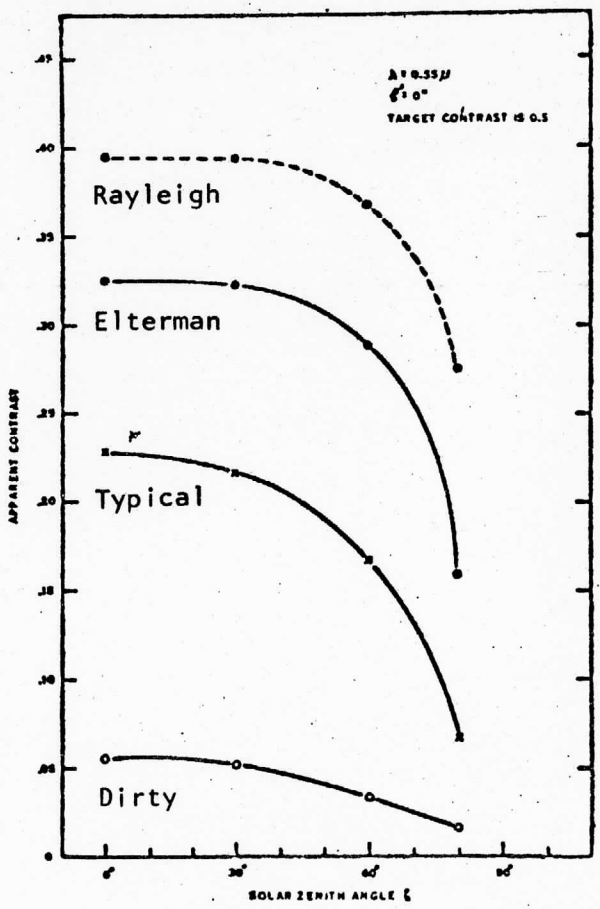

Figure 42

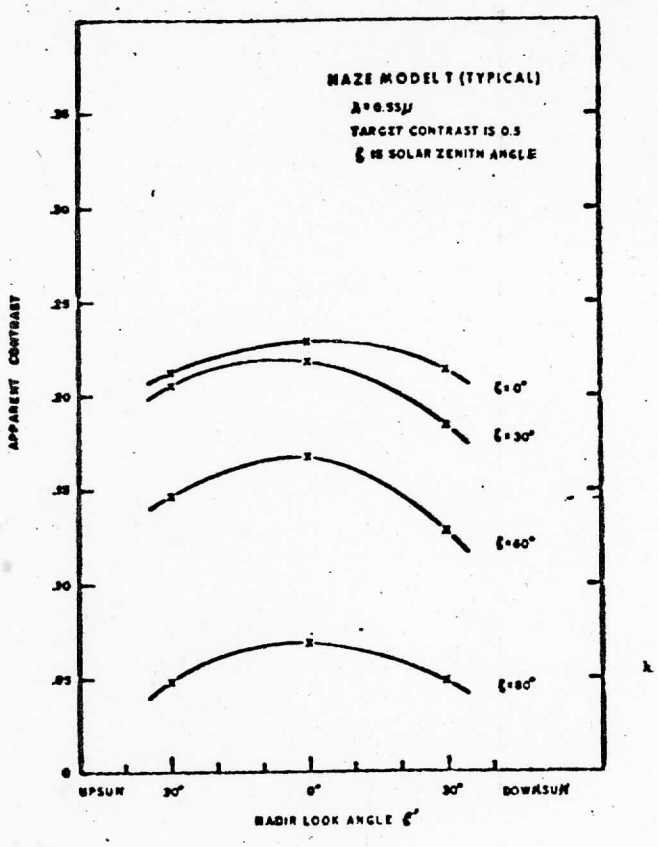

Figure 43

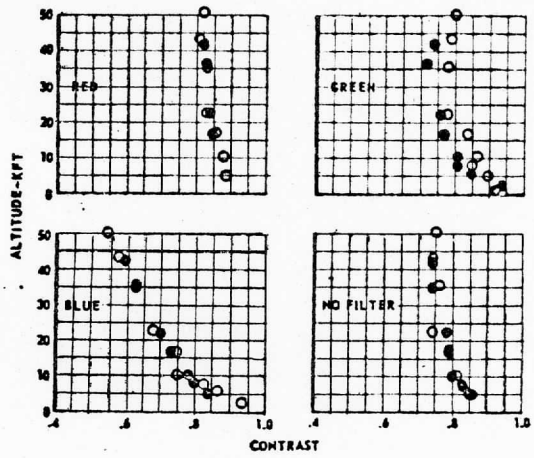

Figure 44

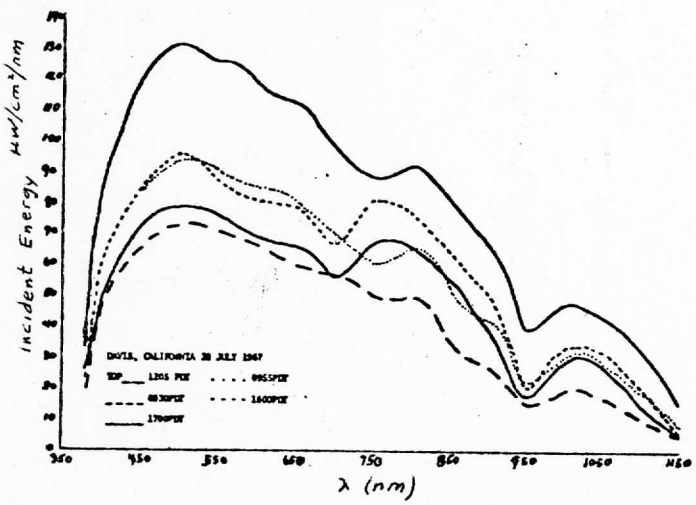

Figure 45

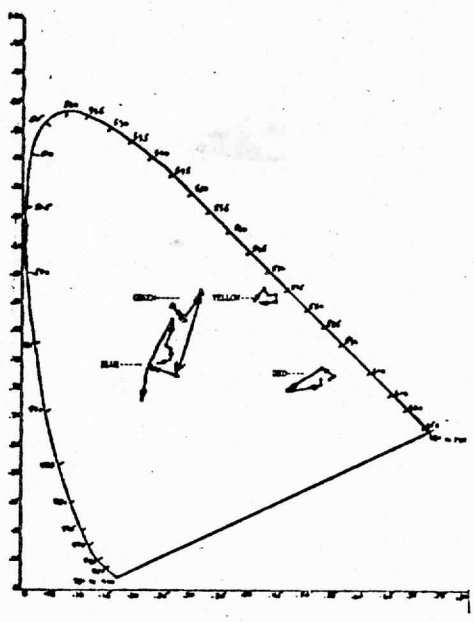

Figure 46

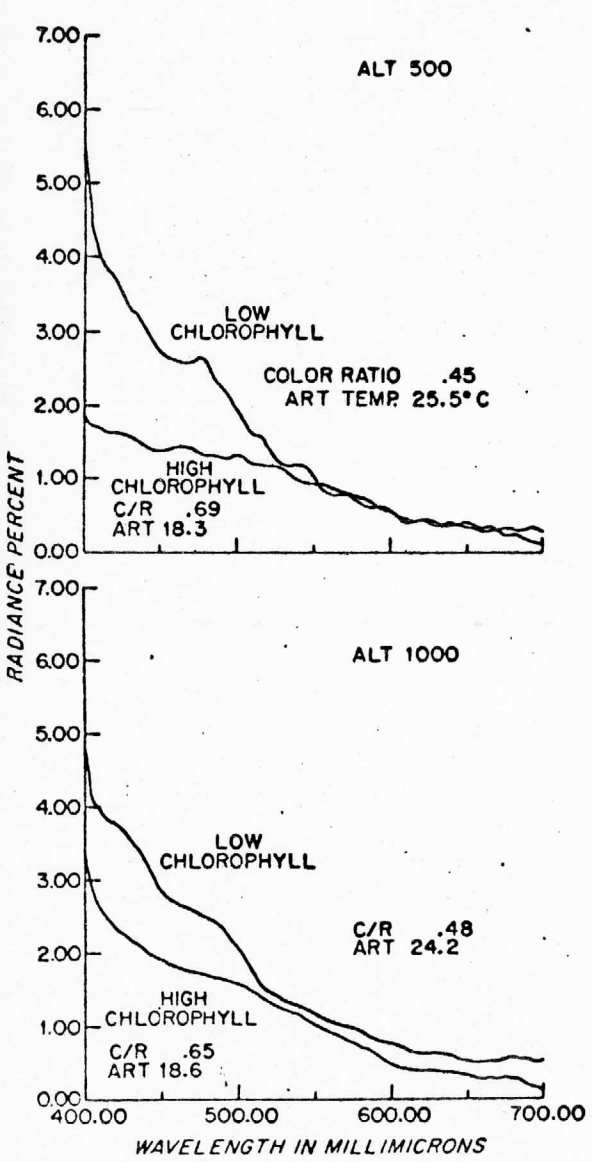
ALT 500
LOW CHLOROPHYLL
COLOR RATIO .45
ART TEMP 25.5°C
HIGH CHLOROPHYLL
C/R .69
ART 18.3
ALT 1000
LOW CHLOROPHYLL
C/R .48
ART 24.2
HIGH CHLOROPHYLL
C/R .65
ART 18.6
RADIANCE PERCENT
WAVELENGTH IN MILLIMICRONS
0.00
1.00
2.00
3.00
4.00
5.00
6.00
7.00
400.00
500.00
600.00
700.00

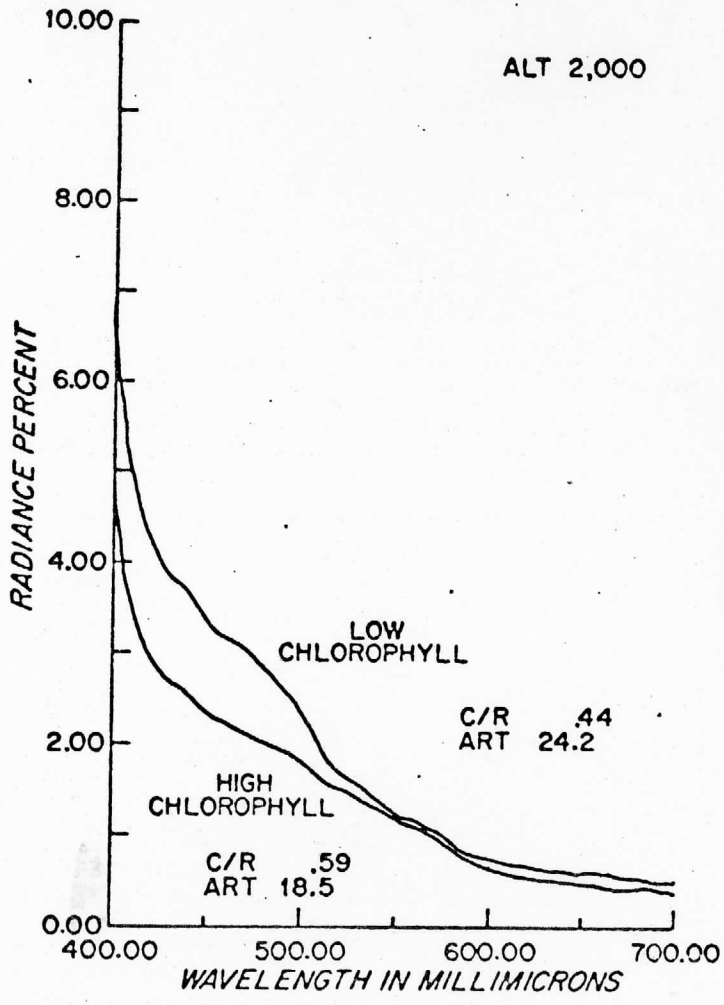
ALT 2,000
LOW CHLOROPHYLL
C/R .44
ART 24.2
HIGH CHLOROPHYLL
C/R .59
ART 18.5
RADIANCE PERCENT
WAVELENGTH IN MILLIMICRONS
0.00
2.00
4.00
6.00
8.00
10.00
400.00
500.00
600.00
700.00

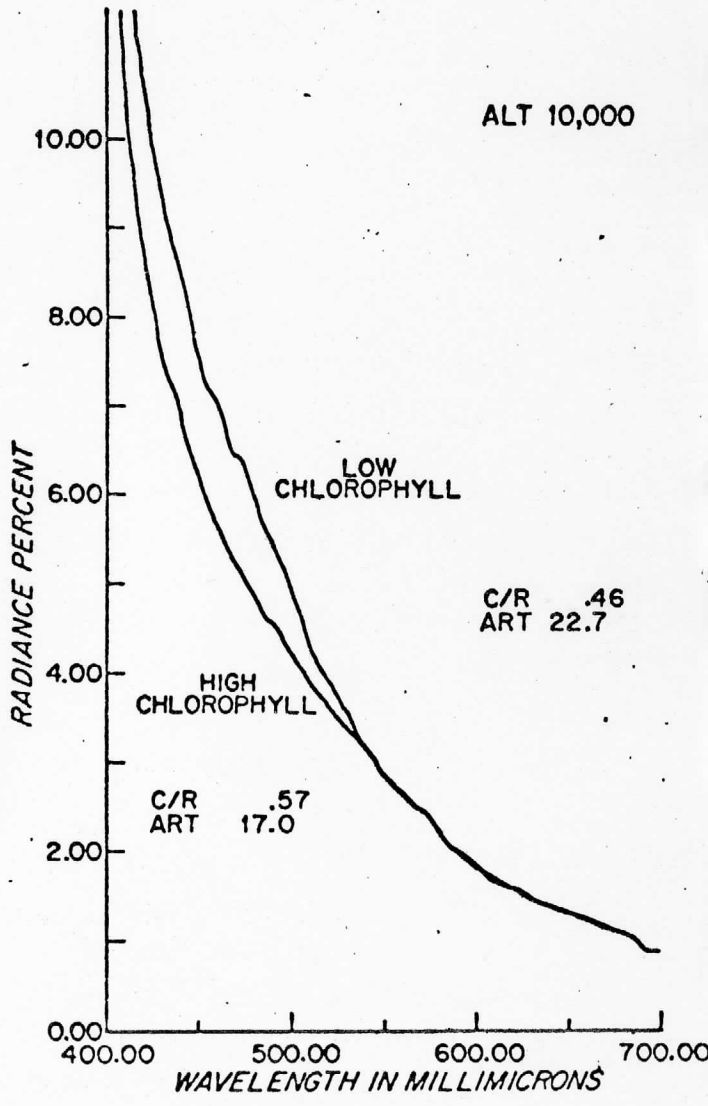
ALT 10,000
LOW CHLOROPHYLL
C/R .46
ART 22.7
HIGH CHLOROPHYLL
C/R .57
ART 17.0
RADIANCE PERCENT
WAVELENGTH IN MILLIMICRONS
0.00
2.00
4.00
6.00
8.00
10.00
400.00
500.00
600.00
700.00

Figure 47

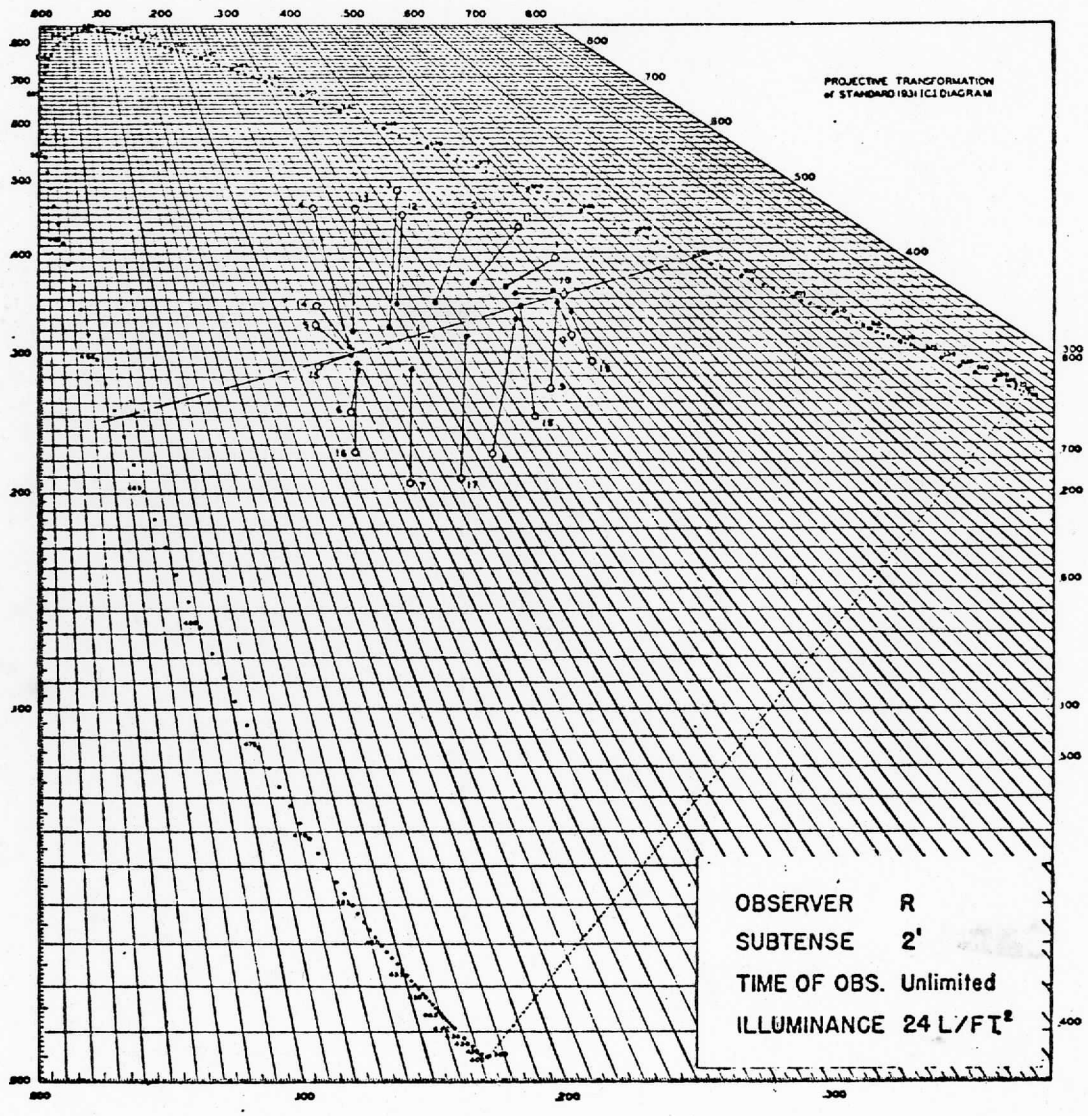
PROJECTIVE TRANSFORMATION
of STANDARD 1931 ICI DIAGRAM
OBSERVER R
SUBTENSE 2'
TIME OF OBS. Unlimited
ILLUMINANCE 24 L/FT²

Figure 48